Lawrence Berkeley National Laboratory

Title
ISOMERISM IN 85At212

Permalink
https://escholarship.org/uc/item/4947m47g

Author
Jones, W. Barclay.

Publication Date
1964-02-03

University of California

Ernest O. Lawrence Radiation Laboratory

ISOMERISM IN $_{85}$At^{212}

Berkeley, California

DISCLAIMER

UNIVERSITY OF CALIFORNIA

Lawrence Radiation Laboratory
Berkeley, California

ISOMERISM IN $_{85}\text{At}^{212}$

W. Barclay Jones

(Ph.D. Thesis)

February 3, 1964

ISOMERISM IN $_{85}At^{212}$

Contents

ISOMERISM IN $_{85}\text{At}^{212}$

William Barclay Jones

Lawrence Radiation Laboratory
University of California
Berkeley, California

February 3, 1964

ABSTRACT

Experiments are reported on the study of $\text{Bi}^{209}(\alpha,n)\text{At}^{212}$ for alpha energies from 15 to 26 MeV. Isomers of At^{212} were found with half lives of 0.118 sec and 0.305 sec decaying to Bi^{208} by alpha emission with alpha energies of (7.66, 7.60 MeV) and (7.88, 7.82 MeV). The energy-level assignments and the half life schematics are discussed in terms of the shell model. The excitation functions were measured and are correlated to compound-nuclear theory.

I. INTRODUCTION

The products formed by bombarding bismuth with alpha particles of many energies have been studied by many investigators.[1-8] To date only limited results have been reported on the reaction $Bi^{209}(\alpha,n)At^{212}$.[6-8] Only limited excitation functions for this reaction have been measured,[8] the modes of decay have not been analyzed completely, the half-life of the isomer of At^{212} has not been reported, and no energy levels for At^{212} have been proposed. The purpose of this investigation is to accumulate experimental data to contribute to the understanding of the nuclear energy levels in this mass region.

A. Compound Nucleus

The compound-nucleus theory of Bohr states that certain nuclear reactions occur in two steps;[9] firstly, the formation of a compound system and, secondly, the breakup of this compound system. These are considered to be independent processes. Thus, we can designate a nuclear reaction by the sequence

$$A + B \rightarrow E^* \rightarrow C + D ,$$
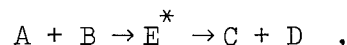
where the nucleus E^* is the compound nucleus. The original projectile loses its identity, and its energy is shared throughout the nucleus. However, the properties of angular momentum, linear momentum, and parity must be conserved. The compound nucleus, E^*, can de-excite by emission of particles or gamma rays; the mode selected depends upon the density of final states, barrier penetrabilities, and the matrix elements of the transition. Ghoshal[10] and John[11] found that the compound-nucleus theory is valid in the region of copper and lead, respectively.

B. Compound Nucleus and Angular Momentum

The excitation energy of the compound-nuclear state and the subsequent sharing of that energy by the products depend upon the kinetic energy of the projectile. There have been many investigations dealing

with the effects of angular momentum upon both neutron and γ-ray emission from an excited nucleus.[12-17] Classically, one can consider the compound nucleus as being put into rotation by the projectile so that the excitation energy, which is provided by the projectile and the Q of the reaction, is put partly into rotational and partly into particle excitation. The energy available for particle emission is therefore the total excitation energy of the nucleus minus the energy of rotation.[18] In the simplest theory of the de-excitation of the compound nucleus, it is assumed that when a compound nucleus has an excitation energy greater than the neutron binding energy, a neutron is emitted. The measured average neutron kinetic energy[19] is much less than the binding energy, so the effect of neutron emission is to remove much thermal energy and very little angular momentum. Hence, successive neutron evaporations leave the compound nucleus with much reduced excitation energy but almost unchanged angular momentum (1/2 $\hbar$ angular momentum change per neutron as a minimum). If there are only a few states of high angular momentum at low excitation energy, then the process of neutron evaporation to these states may be so slowed down that de-excitation by γ-ray emission becomes more probable. This causes the observed shift of excitation functions for these high angular-momentum states toward higher particle energy. We apply these theories to our results.

C. Nuclear Isomerism

Nuclear isomerism was first observed by Hahn in 1921 for the isomeric pair uranium X_2 ($_{91}Pa^{234}$) and uranium Z ($_{91}Pa^{234}$).[20] Both have atomic number 91 and mass number 234, but their radioactive properties are widely different. Although UX2 and UZ had been known for many years, the phenomenon of nuclear isomerism did not receive much attention until another pair of isomers, Br^{80}, was discovered among artificially produced radioactive species in 1937.[21] At that time, Von Weizsacker[22] gave a theoretical explanation of isomerism. He proposed that a nuclear isomer was a metastable excited state in a nucleus. In general, isomerism is said to exist if states other than the ground state can be detected as

separate entities. We assume that as the ability to measure shorter periods of time improves, the number of nuclear excited states classified as isomers will increase. Segrè and Helmholz have outlined various types of isomerism,[23] and we will refer to these types for our own case.

D. Application of Angular-Momentum Effects to Isomeric Cross-Section Ratios

When a pair of isomers is formed as a result of some compound-nucleus reaction, it is found that the ratio of their yields is partly determined by their spins. Using a spin-dependent level-density formula, Vanderbosch and Huizenga were able to account for many of the experimental results.[15] The ratio is also dependent to a smaller extent on the assumed number and multipolarity of the gamma cascade following neutron evaporations. This approach has been used successfully by many other workers.[16,17,24] We will correlate both calculated and experimentally obtained values of the nuclear-spin density parameter to the results of this work.

E. Energy Levels of Odd-Odd Nuclei

Recently there have been several investigations of the spins of odd-odd nuclei near the doubly closed shell of Pb^{208}. In general, one attempts to apply Nordheim's "Strong Coupling" rule for odd-odd nuclei.[25] This rule has been justified theoretically by de-Shalit using a zero-range force between the odd proton and the odd neutron.[26] Calculations for specific odd-odd nuclei have been made by several workers for a finite-range force in which central exchange forces are excluded.[27] Kim and Rasmussen studied several odd-odd nuclei by using a central and the tensor part of the nuclear force, and neglecting the spin-orbit force entirely.[28] Mello and Flores studied Bi^{210} by specifically using a Wigner and Bartlett force plus a tensor interaction.[29] The theoretical approach has been to assume that the doubly closed shell can be treated as an inert core. By treating the core as a source of the central field, a study is made of the extra nucleons outside this core.

Basis vectors are products of the harmonic-oscillator functions for particles 1 and 2, coupled to a total angular momentum:

$$J: |a\rangle = R_1(r_1) R_2(r_2) |j_1 j_2 JM\rangle$$

where $R_1(r_1) R_2(r_2)$ is the radial part of the wave function and $|j_1 j_2 JM\rangle$ is the angular part. If particles 1 and 2 are identical, then the wave function must be antisymmetrized.

The Hamiltonian is assumed to be of the form $H = H_1 + H_2 + V_{12}$, where H_1 and H_2 are the single-particle Hamiltonians, and V_{12} is the residual interaction between the particles. It is further assumed that

$$H_i |a\rangle = \epsilon_0^i |a\rangle ,$$

where ϵ_0^i denotes the single-particle energy for the ith particle.

The sum of the single-particle energies ϵ^1 and ϵ^2 is taken to be the zero-order energy level. It follows that the

$$\left(g_{9/2}, h_{9/2}\right)_{J=0,1,2,3,4,5,6,7,8,9}$$

states lie below all other states such as $\left(i_{11/2}, h_{9/2}\right)$, $\left(g_{9/2}, f_{7/2}\right)$, $\left(d_{5/2}, h_{9/2}\right)$, etc., which can be made by raising the single-particle energies. This assumption appears to be justified in the case of Bi^{210}; however, how far this can be extended is not clear. It is hoped that this approach can be used qualitatively to explain and establish some levels of At^{212}.

F. Alpha-Energy Schematics and Decay-Energy Cycles

The existence of simultaneous alpha and beta instability in the heavy-element nuclide region has made it convenient to utilize energy balances in closed decay-energy cycles to examine the internal consistency of the decay data.[30] However, since the cycles connect only those nuclides differing in mass number by four, there are four sets of closed cycles corresponding to mass types 4n, 4n+1, 4n+2, and 4n+3. Decay energies associated only with the ground-state isomer have been used.

Way and Wood have constructed an alternate energy-balancing system using neutron and proton-binding-energy cycles, which relates neighboring isotopes through experimentally determined Q values.[31] Alpha-decay energies may also be predicted from a plot of the mass number against alpha energy.[32]

We introduce our data into the above schematics and check for inconsistencies.

G. Alpha Decay Rates

In simple alpha-decay theory, the decay constant, λ is determined by the equation $\lambda = fP$, where P is the penetration factor, and f is the reduced transition probability. One can interpret f as the number of collisions per sec with the barrier (frequency factor) and P as the fraction of collisions resulting in transmission. The product of the half life and the penetration factor measure the reciprocal square of the matrix element for alpha decay. Consequently, the hindrance factor, F, of the alpha decay corresponds to the ft value of β decay; the "allowed" transitions of alpha decay are the ground-state transitions of even-even nuclei, which have unity hindrance factor.

Theoretical investigation of alpha decay is beyond the scope of this work but one might consult the work of Gamow, Condon and Gurney,[33] Bethe,[34] Winslow,[35] and Thomas[36] for earlier analyses and, more recently, the work of Mang,[37] Zeh,[38] Rasmussen,[39] Harada,[40] and Preston[41] for the theoretical basis for alpha decay rates. We will use the alpha-decay hindrance-factor empirical equation of Gallagher and Rasmussen[42] for comparison of the excited-state groups to the ground-state transitions to demonstrate the validity of the proposed decay scheme.

II. EXPERIMENTAL PROCEDURES
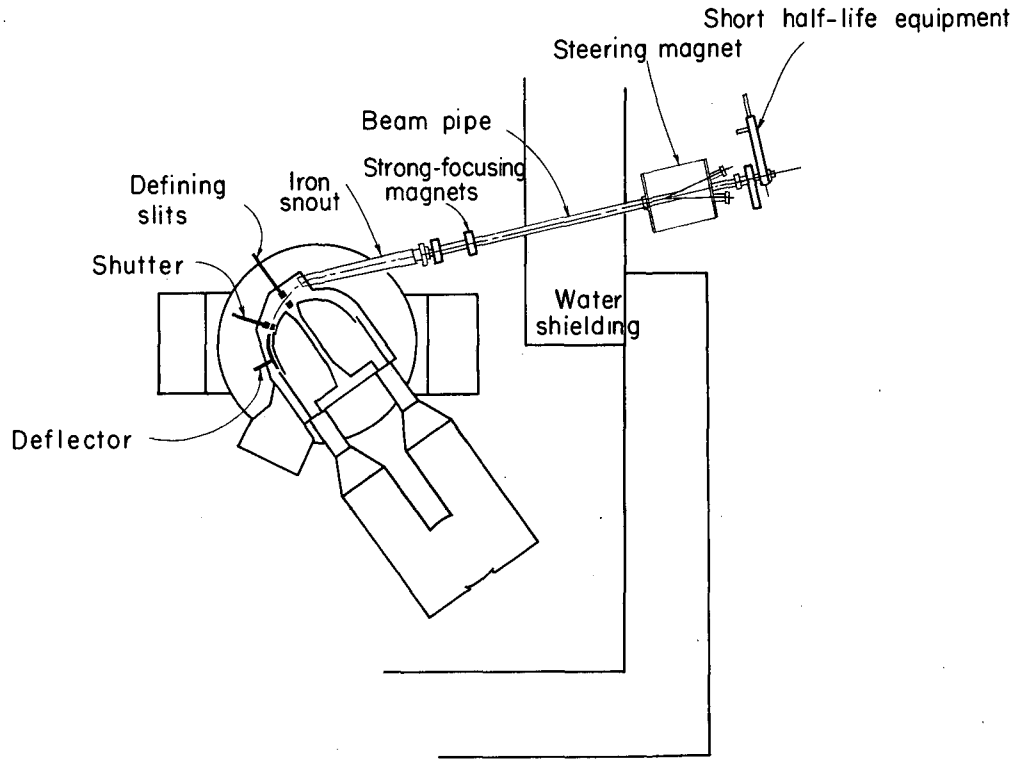
A. 60-Inch Cyclotron Experiments

1. Mechanical Procedure

The study of reactions induced by alpha particles in bismuth targets is simplified since neutron emission is the predominant process. Emission of gamma rays is negligible by comparison, and emission of charged particles is strongly depressed by the Coulomb barrier. Bismuth is very suitable for study because it is monoisotopic, readily obtainable in high purity, and easily evaporated to form thin films. In addition, most of its products are alpha-active, so disintegration rates and energies are easily determined.

Preliminary determinations of the energy of the alpha particles from decay of reaction products in the bismuth target foil resulted in energy values lower than previously reported. This is caused by the compound nucleus's being driven into the foil so that the alpha particle must traverse a certain thickness of bismuth to escape. The alpha particle suffered an energy loss of 100 keV and a straggling which caused a loss in energy resolution. This problem was solved by permitting the reaction products to be driven from the foil by their forward momentum and to be captured by a "recoil catcher," where energy loss and straggling of subsequent alpha emission could be neglected.

The equipment used and the experimental method for focusing the cyclotron beam on a target external to the water shielding has been outlined and described by Fischer[43] and Ellis.[44] Figure 1 shows the experimental layout.

The mechanical apparatus (Fig. 2) used for this experiment consisted of a multiple-foil wheel mounted in front of a welded aluminum vacuum chamber with a gasketed lid. A lucite window was used as a lid to observe the operations of the interior parts while the chamber was evacuated. During the experiments the lid was taped over to make it light-tight.

The mechanical operation consisted of a time sequence as follows. A mechanical shutter, described by Jenkins and Jones,[45] initially in a

Fig. 1. Diagram of experimental arrangement for work
performed at the 60-Inch Cyclotron.
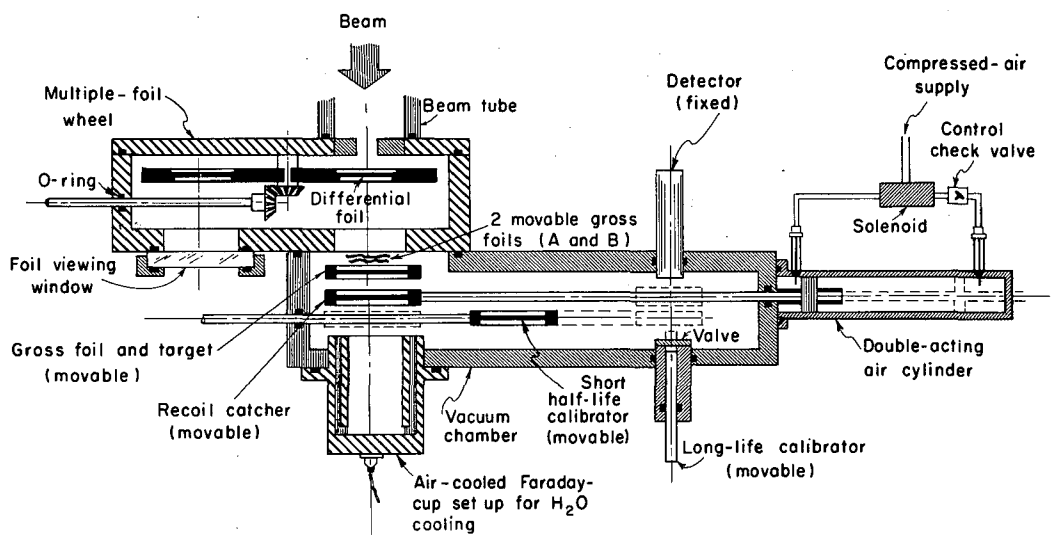
Fig. 2.   Cross section of short-half-life apparatus used for
experimental work at the 60-Inch Cyclotron.

closed position, was opened. Simultaneously, a blocking signal was given to the pulse-height analyzer (PHA), and the recoil catcher was pushed by the air piston, locating it behind the target. After a 0.5-sec bombardment, the shutter was closed, the PHA was unblocked, and the recoil catcher was pulled back to face the detector.

Ports in various locations in the vacuum chamber were used for inserting other parts and equipment. The shaft and flange seals were made with O-rings. The recoil catcher was moved back and forth in a track by a double-acting air cylinder. The air supply to the cylinder was regulated by a control check-valve, permitting an adjustable range of target ejection forces and velocities.

The chamber contained two energy-degrading foils (A and B) which could be interposed independently between the foil wheel and the target. The target foil was an 128.4-mg/cm^2 aluminum absorber with 0.1 mg of bismuth evaporated on it over an area of 5.06 cm^2, the bismuth side facing the Faraday cup. The recoil catcher was 0.5-mil mylar film. The detector was a guard-ring phosphorus-diffused silicon detector as described by Goulding and Hanson.[46] A Th^{228} source could be presented to the detector so as to calibrate the electronic equipment. The Faraday cup was similar to that described by Ellis. Table 1 gives the range of energies available for investigation.[47]

Figure 3 shows the time sequence. The solenoid driving the recoil catcher delayed approximately 30 ms, and the catcher took 60 ms to make the trip. Consequently, the time sequence was so slow that it was difficult to interpret results. These problems were corrected in other experiments described below.

2.   Electronics

The initial research was started using a CsI crystal viewed by a Dumont 6292 photomultiplier tube operated at 1100 V. The crystal was a 1/4-inch diameter and 150 mg/cm^2 thick. The resolution was 600 keV for full width at half maximum (FWHM). This did not permit evaluation of the energy of alpha emission of At^{212} nor the excitation functions for the nuclear reaction, and the experiment was discontinued.

Table I. Incident-particle energies at the 60-Inch Cyclotron. The total range of the beam is 233.0 mg/cm^2.

Foil	Foil-wheel thickness (mg/cm^2)	Total absorber thickness (mg/cm^2)	Remaining beam range (mg/cm^2)	Particle energies (MeV)	Foil	Foil-wheel thickness (mg/cm^2)	Total absorber thickness (mg/cm^2)	Remaining beam range (mg/cm^2)	Particle energies (MeV)
0-0	0	128.4	104.6	30.2	B-0	0	148.3	84.7	26.8
0-1	3.66	132.1	100.9	29.6	B-1	3.66	152.0	81.0	6.15
0-2	7.25	135.7	97.3	29.0	B-2	7.25	155.6	77.4	25.45
0-3	10.9	139.3	93.7	28.4	B-3	10.9	159.2	73.8	24.7
0-4	12.96	141.4	91.6	28.05	B-4	12.96	161.3	71.7	24.3
0-5	16.62	145.0	88.0	27.4	B-5	16.62	164.9	68.1	23.6
0-6	20.21	148.6	84.4	26.75	B-6	20.21	168.5	64.5	22.9
0-7	23.87	152.3	80.7	26.1	B-7	23.87	172.2	60.8	22.1
0-8	25.92	154.3	78.7	25.7	B-8	25.92	174.2	58.8	21.65
0-9	29.58	158.0	75.0	25.0	B-9	29.58	177.9	55.1	20.9
0-10	33.17	161.6	71.4	24.25	B-10	33.17	181.5	51.5	20.05
0-11	36.83	165.2	67.8	23.55	B-11	36.83	185.1	47.9	19.2
A-0	0	167.2	65.8	23.15	AB0	0	187.1	45.9	18.7
A-1	3.66	170.9	62.1	22.4	AB1	3.66	190.8	42.2	17.85
A-2	7.25	174.5	58.5	21.6	AB2	7.25	194.4	38.6	16.9
A-3	10.9	178.1	54.9	20.85	AB3	10.9	198.0	35.0	15.95
A-4	12.96	180.2	52.8	20.35	AB4	12.96	200.1	32.9	15.3
A-5	16.62	183.8	49.2	19.5	AB5	16.62	203.7	29.3	14.35
A-6	20.21	187.4	45.6	18.65	AB6	20.21	207.3	25.7	13.25
A-7	23.87	191.1	41.9	17.7	AB7	23.87	211.0	22.0	12.0
A-8	25.92	193.1	39.9	17.2	AB8	25.92	213.0	20.0	11.3
A-9	29.58	196.8	36.2	16.3	AB9	29.58	216.7	16.3	10.0
A-10	33.17	200.4	32.6	15.25	AB10	33.17	220.3	12.7	8.5
A-11	36.83	204.0	29.0	14.25	AB11	36.83	223.9	9.1	6.85
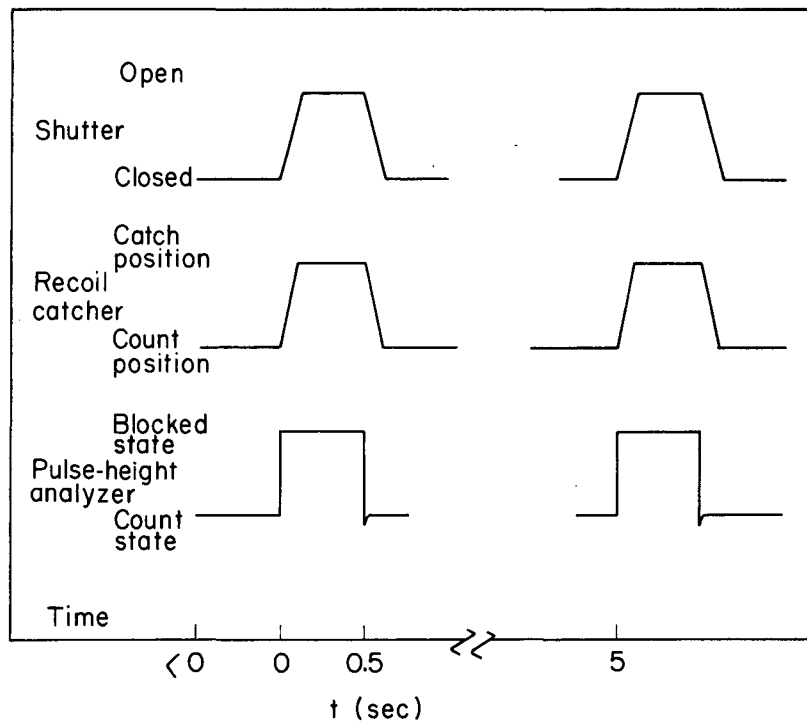
Fig. 3. Diagram of time sequence for work performed at the 60-Inch Cyclotron.

With the development of semiconductor detectors, a phosphorous-diffused-junction, p-n (guard-ring) detector with a resolution of 35 keV (FWHM) was used. Figure 4 is the block diagram of the counting equipment used for pulse-height analysis.

When the alpha particle was detected by the semiconductor detector, the pulse was amplified by the preamplifier to $\sim$ 1 V and then sent through $\sim$ 70 ft of RG63U cable to the counting area. Here it was amplified in a MOD-VI linear amplifier[48] and then presented to a 400-channel PHA for analysis. It was with this equipment that the 35-keV (FWHM) resolution was obtained; the system was calibrated with a Th^{228} source which was isolated from the vacuum chamber by a valve. The residual activity, which remained in the chamber for 4 or 5 days after calibration was used as a monitor for long-term drifts of the system.

The sequence of operations was as previously described. A Tektronix 543 oscilloscope was set to sweep every 5 sec. This sweep initiated a signal in the relay box which sent a + 24 V blocking signal to the PHA, a 110 V ac signal to the control room to initiate the shutter action, and a 110 V ac signal to the target area to activate the air solenoid that drove the recoil catcher over to the target position.

This sequence of controls for the measurement of the excitation functions of the Bi(α,n)At reaction was adequate to look at 0.2-sec or longer half lives, even though there was a 30 to 40 ms jitter in the system as well as a fixed 60-ms delay. However, these uncertainties were burdensome and created an impossible situation when it was found that two half lives were involved in the alpha decay of At^{212}. Unfortunately, the 60-Inch Cyclotron was due for dismantling before this problem could be remedied, so the work was concluded with different equipment and techniques on the 88-Inch Cyclotron. This will be described later.

3. Time Sequence

The sequence of controls for the measurement of half lives was the same as above with the addition of two elements. The signal was not
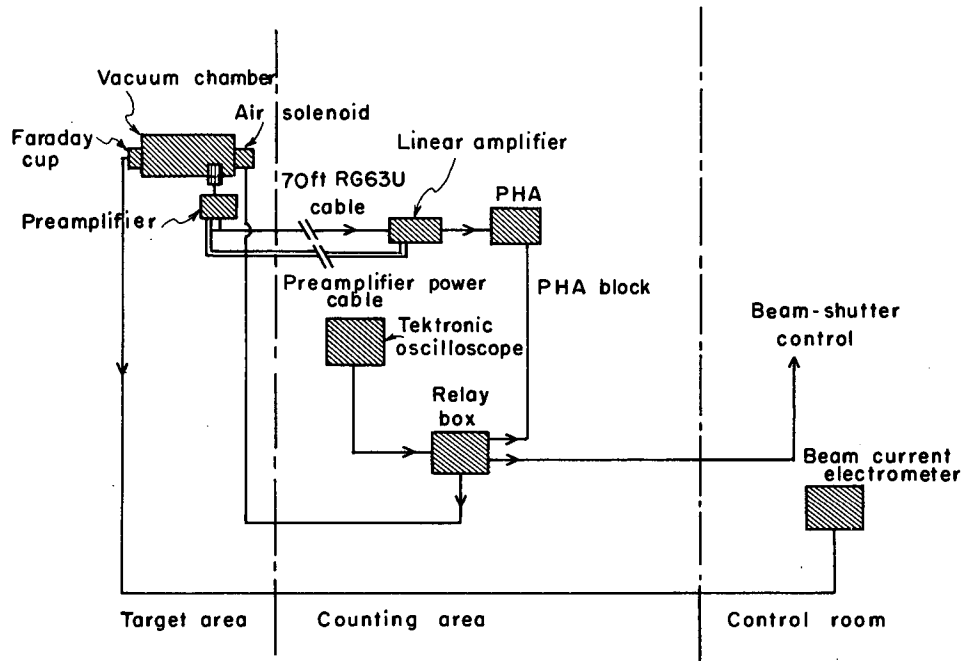
Fig. 4. Equipment location at the 60-Inch Cyclotron.

sent from the linear amplifier to the PHA, but was sent to an upper-lower discriminator (a window) which could be set to deliver a pulse whenever a particle of a chosen energy was detected. This circuit proved to be remarkably stable and maintained itself to within two channels of width for 8-hr periods. For this experiment, two channels were equivalent to 20 keV. Thus, there was no problem for maintaining the window to view only one member of the alpha groups of the decay of At^{212}.

The PHA has a time mode of operation in which it is made to address each channel consecutively by an external pulser. A signal can be presented to the analyzer; this shows as a count in the channel which is being addressed at the time the signal arrives. A Hewlett-Packard No. 524 signal generator was set to deliver a pulse every 16-2/3 ms (60~) or 10 ms. The relay box delivered a reset signal to the PHA which set the address to channel zero at the end of a beam pulse; thus, the PHA started addressing channel after channel every 16-2/3 ms. If particles were detected, a count appeared in the channel being addressed. This operation repeated itself every 5.0 sec, addressing 300 channels. By observing the number of channels addressed, the proper function of the time sequence of the system could be verified.

B. 88-Inch Cyclotron Experiments

1. Mechanical Procedure

The same foil wheel used at the 60-Inch Cyclotron was used. However, a new vacuum chamber and degrading-foil holder were fabricated. The beam was directed through a water-cooled collimator (Fig. 5), past foils A and B, which could be independently interposed in the beam path, and then through the foil wheel. This gave a controlled degradation of the beam energy. The beam then passed through the target foil, which was 7.2 mg/cm^2 of aluminum with 0.1 mg of bismuth evaporated over an area of 5 cm^2 with the bismuth facing the recoil catcher of 0.25-mil mylar film. After passing through the recoil catcher, the beam was collected in a water-cooled Faraday cup. The chamber also contained two ports, one for the
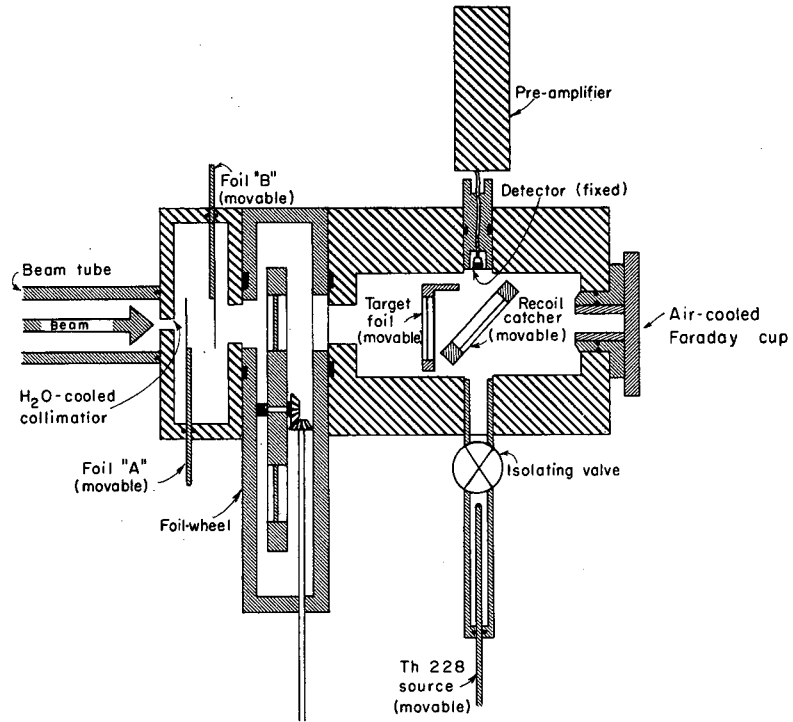
Fig. 5. Cross section of short-half-life apparatus used at 88-Inch Cyclotron.

detector--in this case a gold surface-barrier detector,[49] the other for the Th^{228} source, which could be isolated when not in use.

The extraction and focusing of the beam have been described by Harvey et al.[50] A bending magnet directed the beam into the high-intensity cave through the external-target system described by Wigle,[51] and into the system described above. The apparatus described in the preceding paragraph had its own collimating system; hence, the beam was forced to pass through the target and recoil catcher before being collected in the Faraday cup.

The 88-Inch Cyclotron provides alpha particles of various energies, and an energy of 33 MeV was selected as the initial beam energy.[52] The beam energy then was degraded according to Table II. The 33-MeV energy permitted investigation of the Bi$^{209}(\alpha,n)$At^{212} and Bi$^{209}(\alpha,2n)$At^{211} reactions without a change in accelerator parameters.

2. Electronics

The 88-Inch Cyclotron has an oscillator pulser (Fig. 6) that can be operated to vary the width of the pulse, the repetition rate of the pulse, and the oscillator voltage during a pulse and between pulses. The pulser controls the dee voltage, so that one can set the dee voltage below threshold and then, at a chosen time, increase the dee voltage to permit beam extraction. Figure 7 is an example of this--the upper sweep is the extracted beam delivered to the Faraday cup; the lower is the dee voltage. For the present case, beam pulses of 40-ms and 1.5-sec repetition rate were chosen. The time sequence for the system is shown in Fig. 8. The upper sweep in Fig. 9 is the pulser, the middle is the signal from the MOD VI to the PHA, and the lower is the signal blocking the PHA. Note that the PHA is blocked during the time that the noise level is high, and that there is high noise level during the beam time (Figs. 8 and 9).

The extraordinary load put upon the preamplifier power supply by the large signal during the beam pulse causes the noise signal from the MOD VI to be modulated with the beam pulse envelope. It could have been corrected by using a "stiffer" regulator on the preamplifier. For this experiment, correction was unnecessary because resolution was adequate even though

Table II. Incident-particle energies at the 88-Inch Cyclotron. The total range of the beam is 122 mg/cm^2 and the target thickness is 7.2 mg/cm^2.

| Foil	Foil-wheel thickness (mg/cm^2)	Absorber thickness (mg/cm^2)	Remaining beam range (mg/cm^2)	Particle energy (MeV)	Foil	Foil-wheel thickness (mg/cm^2)	Absorber thickness (mg/cm^2)	Remaining beam range (mg/cm^2)	Particle energy (MeV)
0-0	0	0	114.8	31.95	B-0	0	39.7	75.1	25.0
0-1	3.66	3.0	111.8	31.45	B-1	3.66	42.7	72.1	24.4
0-2	7.25	6.95	107.8	30.8	B-2	7.25	46.7	68.1	23.6
0-3	10.9	9.0	105.8	30.5	B-3	10.9	48.7	66.1	23.3
0-4	12.96	10.1	104.7	30.3	B-4	12.96	49.8	65.0	23.0
0-5	16.62	13.1	101.7	29.8	B-5	16.62	52.8	62.0	22.35
0-6	20.21	17.0	97.8	29.1	B-6	20.21	56.7	58.1	21.5
0-7	23.87	19.5	95.3	28.7	B-7	23.87	59.2	55.6	21.0
0-8	25.92	21.0	93.8	28.4	B-8	25.92	60.7	54.1	20.65
0-9	29.58	22.5	92.3	28.15	B-9	29.58	62.2	52.6	20.3
0-10	33.17	26.5	88.3	27.45	B-10	33.17	66.2	48.6	19.35
0-11	36.83	29.6	85.2	26.95	B-11	36.83	69.3	45.5	18.65
A-0	0	20.2	94.6	28.55	AB-0	0	60.1	54.7	20.8
A-1	3.66	23.2	91.6	28.0	AB-1	3.66	63.1	51.7	20.0
A-2	7.25	27.2	87.6	27.4	AB-2	7.25	67.1	47.7	19.15
A-3	10.9	29.2	85.6	27.0	AB-3	10.9	69.1	45.7	18.7
A-4	12.96	30.3	84.5	26.8	AB-4	12.96	70.2	44.6	18.4
A-5	16.62	33.3	81.5	26.2	AB-5	16.62	73.2	41.6	17.65
A-6	20.21	37.2	77.6	25.5	AB-6	20.21	77.1	37.7	16.5
A-7	23.87	39.7	75.1	25.0	AB-7	23.87	79.6	35.2	16.0
A-8	25.92	41.2	73.6	24.7	AB-8	25.92	81.1	33.7	15.55
A-9	29.58	42.7	72.1	24.4	AB-9	29.58	82.6	32.2	15.15
A-10	33.17	46.7	68.1	23.6	AB-10	33.17	86.6	28.2	14.05
A-11	36.83	49.8	65.0	23.0	AB-11	36.83	89.7	25.1	13.05
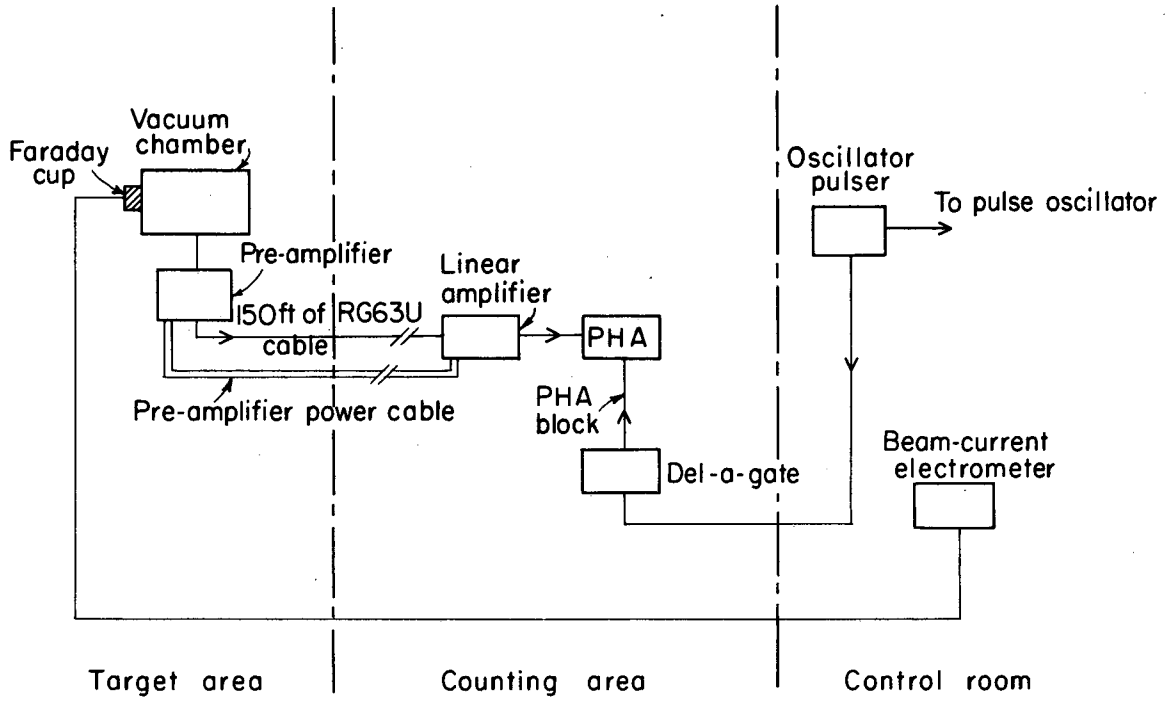
Fig. 6. Sketch showing equipment location for work performed
     at the 88-Inch Cyclotron.
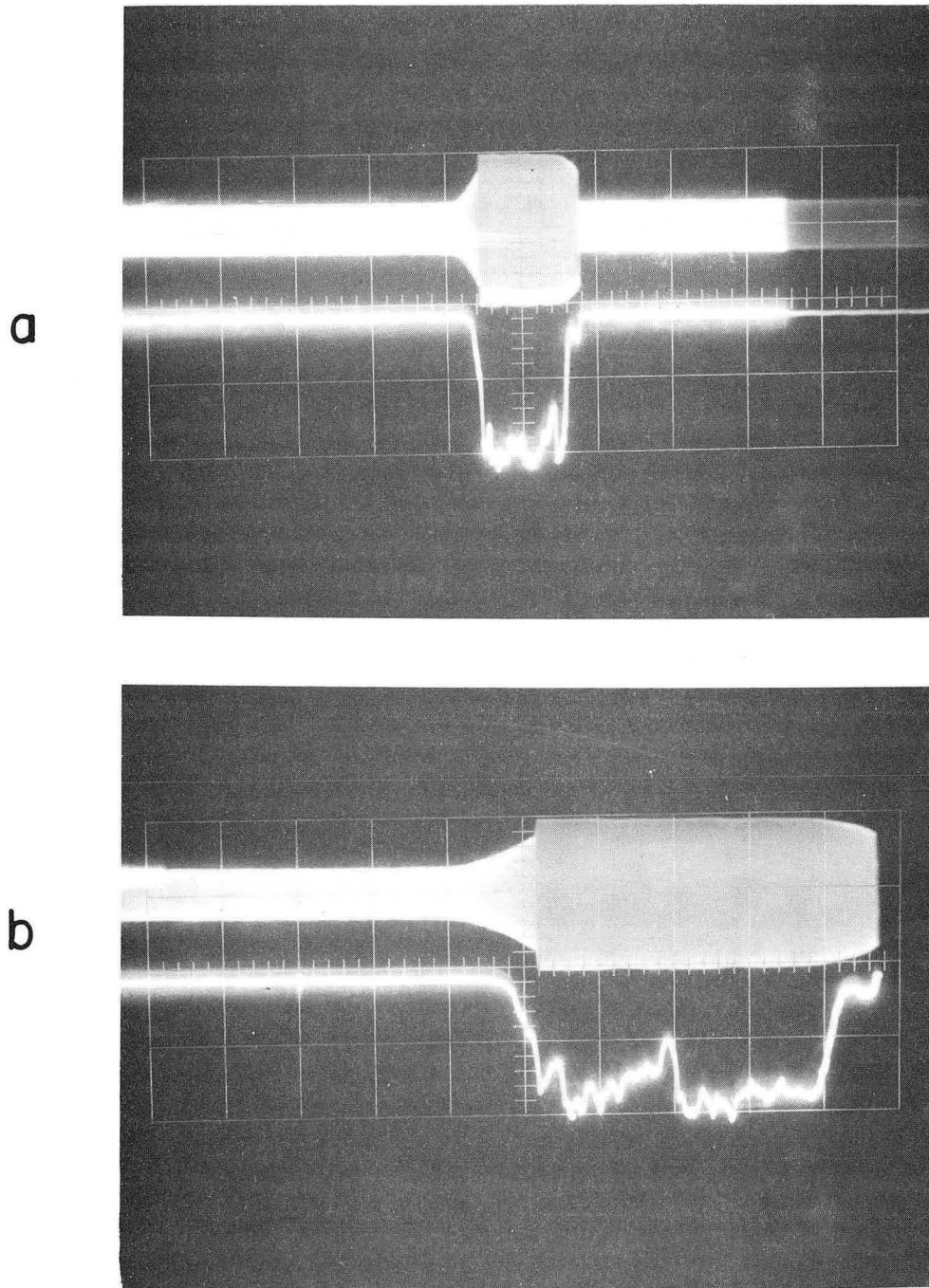
ZN-4180

Fig. 7. Oscillographic picture of the 88-Inch Cyclotron beam
and dee voltage while the cyclotron is pulsed. (a) Sweep
speed is 0.04 sec/cm, beam sensitivity (top trace) is
0.5 μA/cm, and dee-voltage sensitivity is 30 kV/cm. (b)
Sweep speed is 0.01 sec/cm, beam sensitivity (top trace)
is 0.5 μA/cm, and dee-voltage sensitivity is 30 kV/cm.
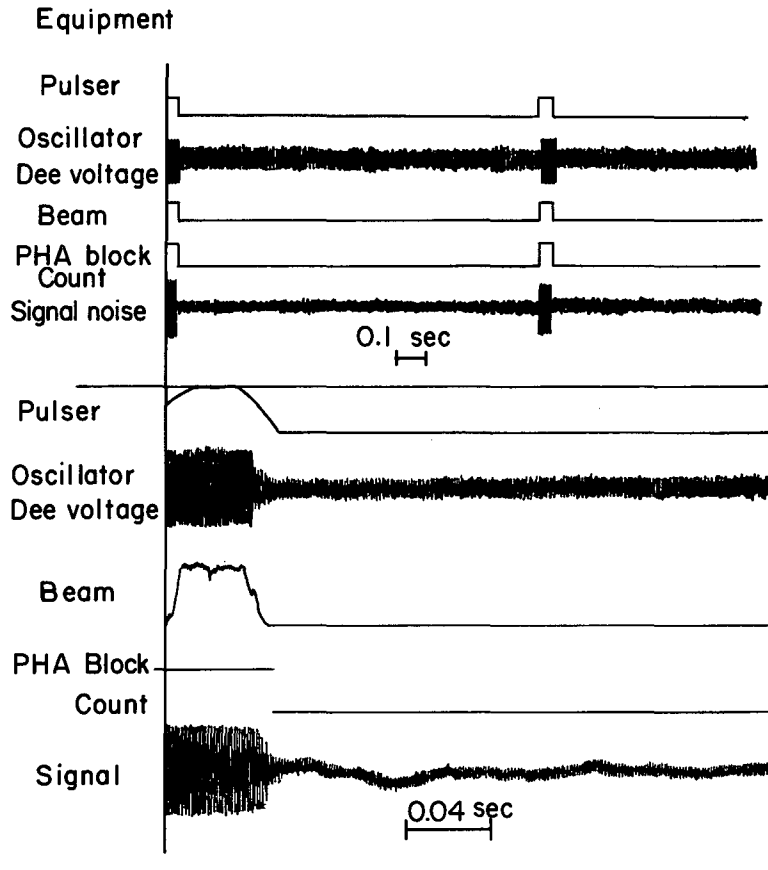
Fig. 8. Diagram of the time sequence of the electronic
equipment at the 88-Inch Cyclotron for this experiment.
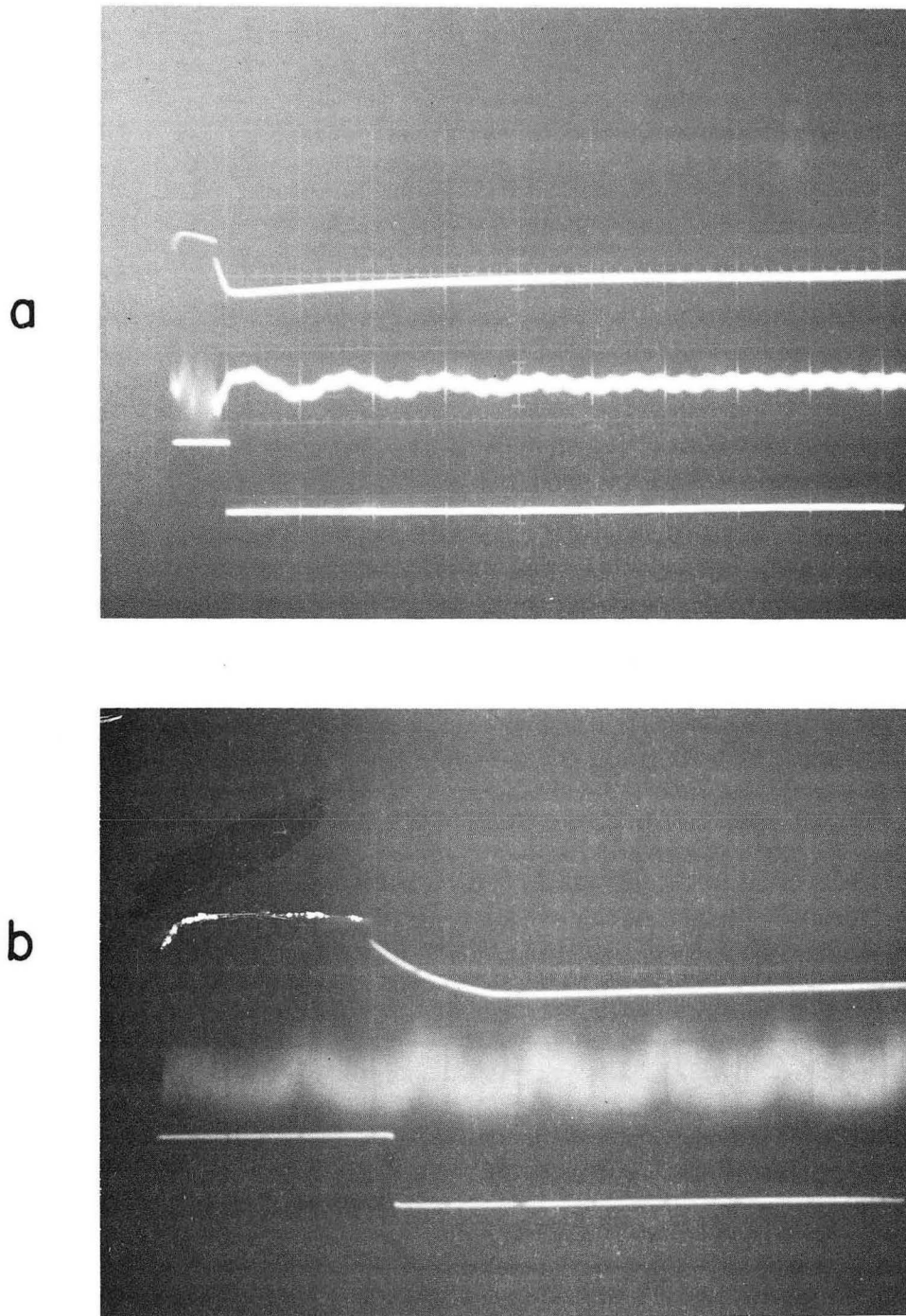
ZN-4181

Fig. 9. Oscillographic picture of pulser, detector signal,
and PHA block at sweep speeds of (a) 50 and (b) 10 msec/cm.
Sensitivities for the traces are 20 V/cm (upper, pulser),
0.05 V/cm (middle, signal), and 5 V/cm (lower, PHA block).

the noise level was raised by a factor of two. However, to relieve some
of the preamplifier overload, the preamplifier was operated on "low"
gain and the MOD VI on "high" gain. This setting does not give quite
as good resolution as the reverse, but it does reduce the drive on the
preamplifier, so that better resolution between beam pulses is obtained.

The gold surface-barrier detector was operated with reverse bias
of 45 V, and the MOD VI amplifier operated with 0.5-μsec rise time and
50-μsec clipping time. The threshold of the amplifier was then set so
the upper 8 V of a 20-V signal (for an 8-MeV alpha particle) was delivered
to the 400-channel PHA.

C. HiLAC Experiments

Experiments were needed to establish the decay modes for At^{212} and
At^{212m} and to find if the only mode of decay of At^{212} is by alpha emission.
Initially, attempts were made to look for gamma de-excitation at the
60-Inch Cyclotron. However, this proved to be impossible with existing
equipment and facilities because the background due to degrading foils
and the Faraday cup and collimators was far in excess of the activity
induced in the bismuth. In general, these materials were of much lower
Z than bismuth, and as the beam energy was just below the Coulomb barrier
for bismuth, it was above the Coulomb barrier for lighter elements.
Therefore their induced activity far exceeded that of bismuth. Accordingly
it was decided to study the gamma de-excitation schematics by searching
for the conversion electrons at the HiLAC.

The Lawrence Radiation Laboratory HiLAC was the source of the 23-MeV
alpha beam. The beam energy is usually 41.5 MeV, but can be varied by
changing the tilt of the gradient of the post-stripper tank and adjusting
the tuners to cause the beam to fall out of phase and to coast the rest
of the way down the tank.[53] The spectrometer used is described fully by
Elbek and Nakamura,[54] and the bombardment arrangement is described by
Diamond et al.[53] The target, bismuth melted on a gold disc, was mounted
at a grazing incident angle to the beam and almost perpendicular to the
electron-detection direction. It was a target relatively thick to the

beam but thin for the electrons. No conversion electrons were found (a cross section of less than 1 mb) from 100 to 800 keV. At the time of this investigation, the equipment was unable to detect electrons of less than 100 keV, but in a subsequent irradiation by Diamond and Stephens, conversion electrons (produced with a cross section greater than 100 mb) were seen, corresponding to a gamma ray of 60 keV.[55] The latter authors were able to determine that the conversion electrons came from bismuth by measuring the L-to-M spacing. However, the LI/LII/LIII ratio was not obtained so that the multipolarity of the gamma de-excitation could not be determined. They made a rough half-life determination of approximately 0.13 sec.

III. EXPERIMENTAL RESULTS

A. Alpha-Decay-Energy Determination

The decay energies of the isomeric states of At^{212} were determined by electronic equipment previously calibrated with a standard alpha source. Th^{228} was introduced into the vacuum chamber in the manner described in the procedure sections. Astatine-211 produced by the $(\alpha,2n)$ reaction is also an excellent calibration source, having two prominent alpha peaks at 5.86 and 7.43 MeV.[6]

Table III shows that the maximum drift of the position of the alpha-particle peak was less than 1.5 PHA channels, which corresponds to approximately 15 keV. This was a long-time drift from bombardment to bombardment; however, the average drift during the course of a single bombardment was less than 0.5 channel, so the results could be interpreted with a 5-keV maximum uncertainty. Using this as a criterion, we have the following results:

Kinetic energy of α-particles	Alpha-decay energy
7.60±.010 MeV	7.78±.010 MeV
7.66±.010 MeV	7.84±.010 MeV
7.82±.010 MeV	8.00±.010 MeV
7.88±.010 MeV	8.06±.010 MeV

The decay energy[42] is the sum of the alpha-particle energy, the recoil energy of the residual nucleus, and the orbital electron "screening" correction. The recoil energy of the residual nucleus equals the product of the mass and energy of the alpha particle divided by the mass of the recoiling nucleus. The orbital electron "screening" correction is

$$\Delta E_{sc} = 65.3(Z + 2)^{7/5} - 80(Z + 2)^{2/5}.$$

An alpha-particle spectrum plotting counts against PHA channel number is given in Fig. 10. The straight line represents pulse height versus energy as calibrated by the Th^{228} alpha source. The scale's accuracy is verified from the At^{211} and Po^{211} peaks. Figure 11 presents

Table III. Alpha-emission energies of At^{212} for various bombardments performed at the 88-Inch Cyclotron.

Run No.	PHA channel of peak Po^{211}	At^{212} peaks 1	2	3	4	Corresponding alpha energy Po^{211}	At^{212} peaks 1	2	3	4
2	---	252.5	258	274	280.5		7.605	7.66	7.825	7.89
4	235	252	257.5	273.5	278.8	7.43[a]	7.60	7.655	7.82	7.875
6	235	252.5	258.2	273.5	279.2	7.43	7.605	7.663	7.82	7.878
9	235	251.5	257.8	273.3	279.6	7.43	7.595	7.66	7.817	7.88
10	235	252	257.5	273.3	279.5	7.43	7.60	7.657	7.817	7.88
11	235.7	251.5	258.0	274.0	280	7.43	7.59	7.655	7.815	7.875
12	235.7	---	258	274	280	7.43	---	7.655	7.815	7.875
13[b]	236	252	258.3	273.7	280.5	7.43	7.598	7.66	7.815	7.88
14[b]	235.5	251.5	257.7	273.5	279.5	7.43	7.60	7.66	7.82	7.88
16	234.7	---	---	---	---	7.43	---			

a. Used as standard (see reference 63).
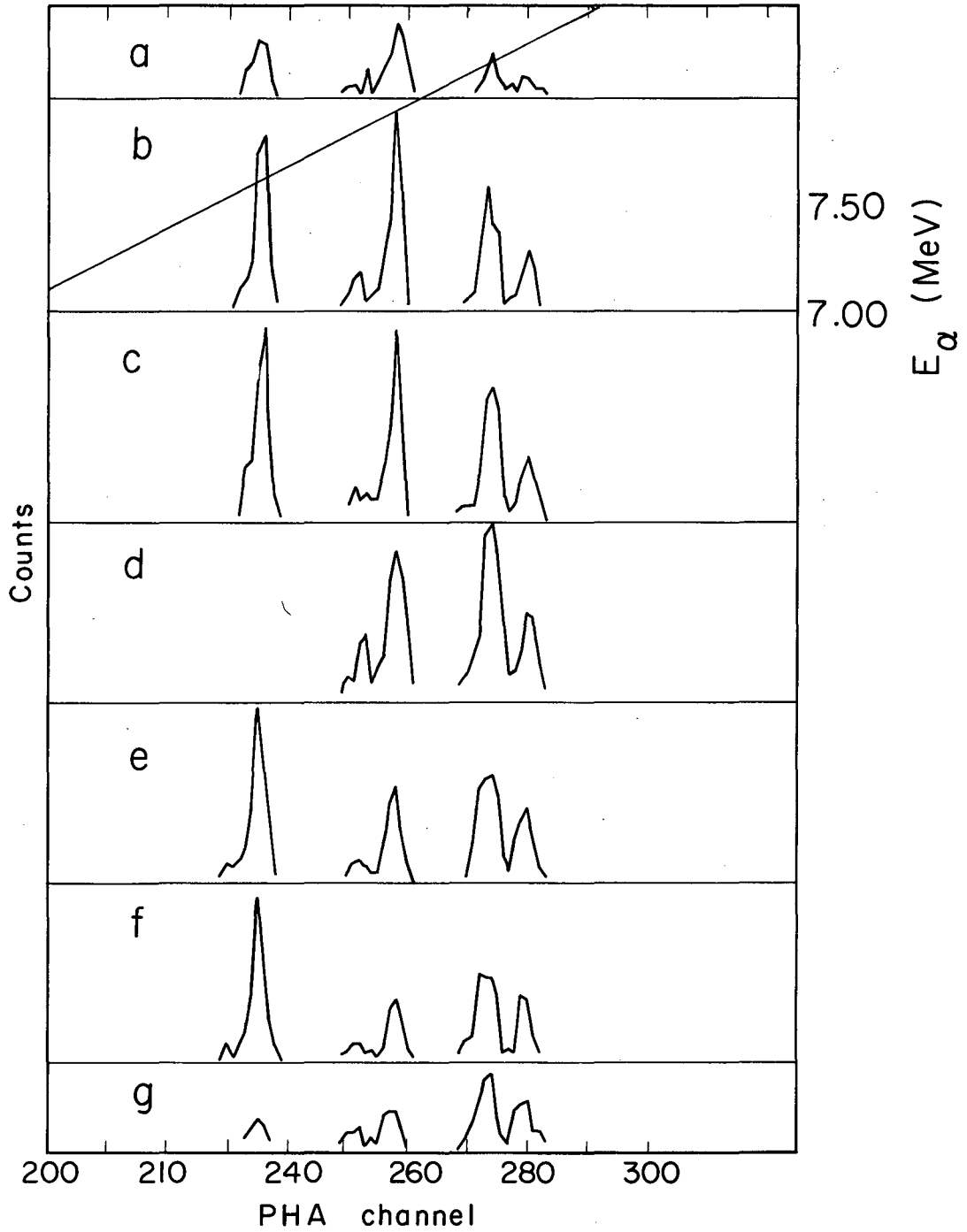
b. Best statistics.
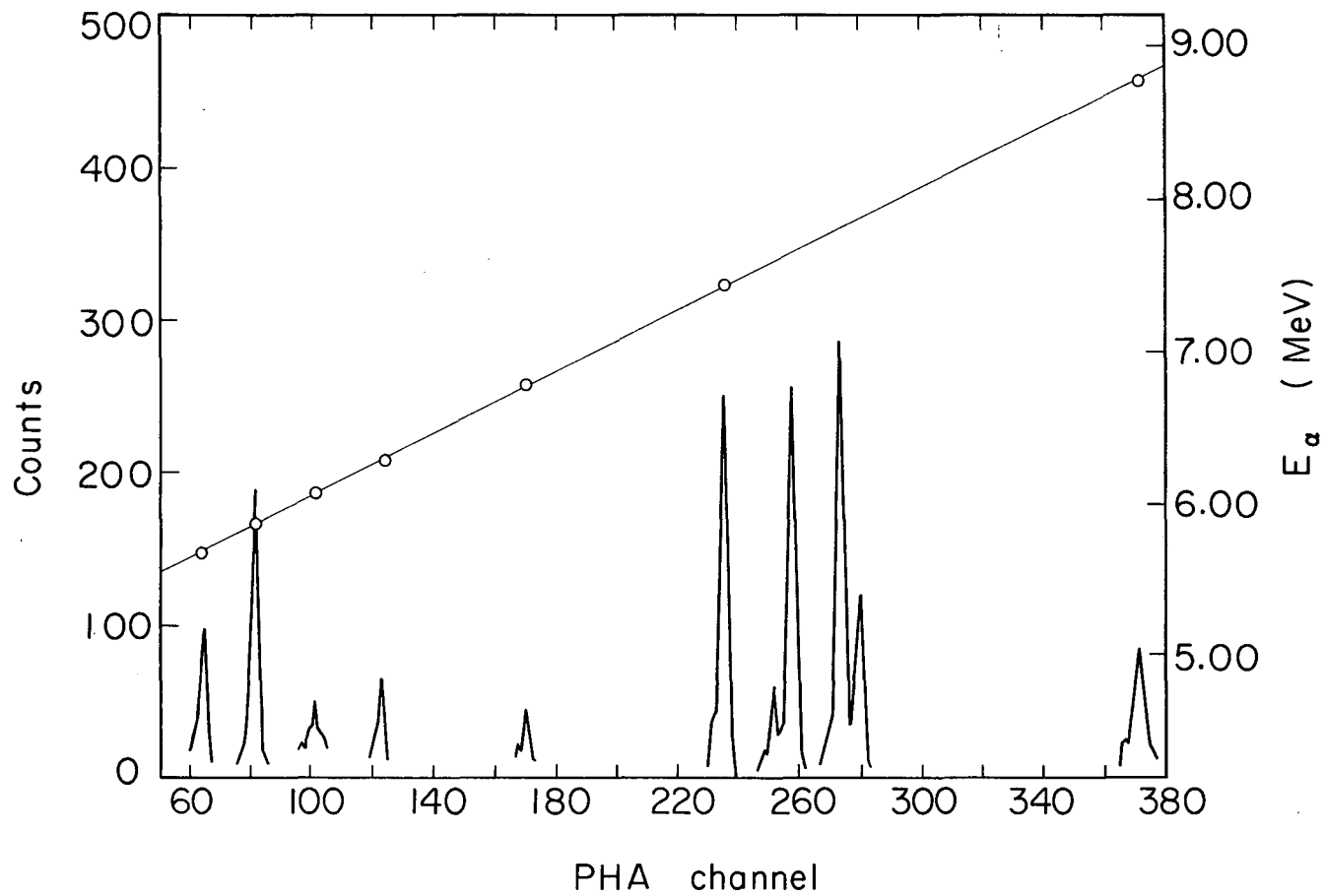
MUB-2474

Fig. 10. Graph of counts versus pulse-height-analyzer channel
    number showing the total alpha spectra for Th^{228}, At^{211},
    Po^{211}, and At^{212}.

Fig. 11. Alpha spectra obtained for incident-particle energies
of (a) 20.3 MeV, (b) 22.15 MeV, (c) 22.5 MeV, (d) 23.0 MeV,
(e) 23.15 MeV, (f) 24.4 MeV, and (g) 25.0 MeV.

MUB-2475

alpha-energy spectra from 7 to 8 MeV for different bombarding energies of the incident helium ions for the same integrated beam. Figures 12 and 13 present alpha spectra for 22.15- and 31.3-MeV incident helium-ion energies for many times more accumulated beam than the spectra shown in Fig. 11.

B. Half-Life Determinations

Initially, an attempt was made to find the half life of At^{212} by the time-sequence mode as described in this paper, without discrimination as to alpha-particle energy. The results indicated that the half life was 0.2 sec, as had been reported previously[6,7,8] (in Fig. 14 however, there appears to be a long-lived tail to this decay). Where the half life of each alpha energy was measured individually, the results appeared as in Figs. 15, 16, and 17.

Peierls has outlined a method of analysis for determining exponential coefficients for radioactive decay.[56] He has shown that the radioactive decay constant λ can be obtained by selecting a time interval Δt which is less than one-third the mean life τ yet is long enough to contain a statistically significant number of counts. Thus, in a continuous sequence of n contiguous equal time intervals of Δt, a total number of counts $x_1, x_2, \cdots x_n$, due to the source pluse background is observed. Therefore we have $\Delta N_1 = x_1 - b\Delta t$, $\Delta N_2 = x_2 - b\Delta t$, etc., where $b\Delta t$ is the expectation value of the number of background counts in time Δt.

The total lifetimes of all atoms that decay between $t = 0$ and $t = n\Delta t$ are $\Delta N_1 (1/2 \, \Delta t) + \Delta N_2 (3/2 \, \Delta t) + \Delta N_3 (5/2 \, \Delta t) + \cdots \Delta N_n [(2n-1)/2]\Delta t$. The total number of atoms observed is $N = \Delta N_1 + \Delta N_2 + \cdots \Delta N_n$. Thus, the average life is

$$s = \frac{[\Delta N_1 + 3\Delta N_2 + 5\Delta N_3 + \cdots \frac{(2n-1)}{2} \Delta N_n]}{\Delta N_1 + \Delta N_2 + \Delta N_3 + \cdots \Delta N_n} \frac{\Delta t}{2} \, .$$

However, those atoms surviving beyond $T = n\Delta t$ are not included, and so the average life is less than the true mean life, τ.
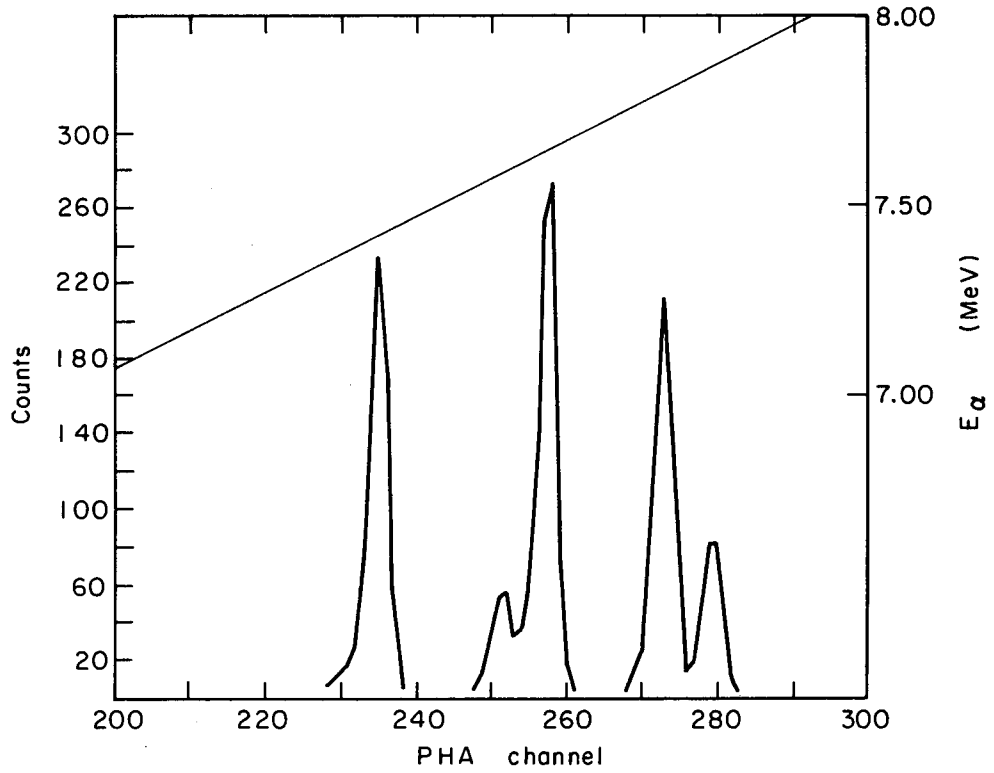
MU-33581

Fig. 12. Alpha spectrum obtained for an incident-particle
energy of 22.15 MeV.
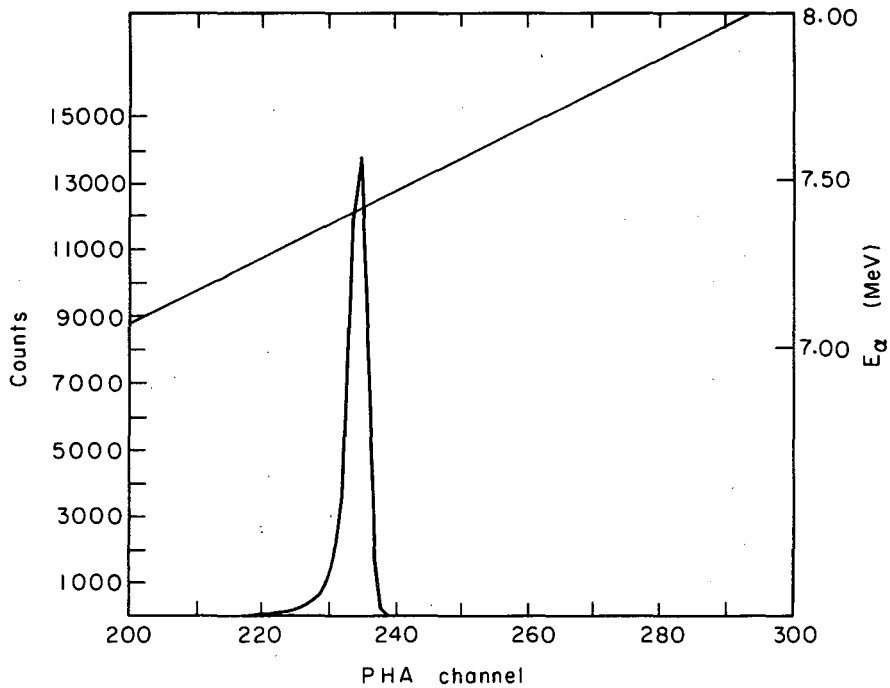
Fig. 13.   Alpha spectrum obtained for an incident-particle
energy of 31.3 MeV.
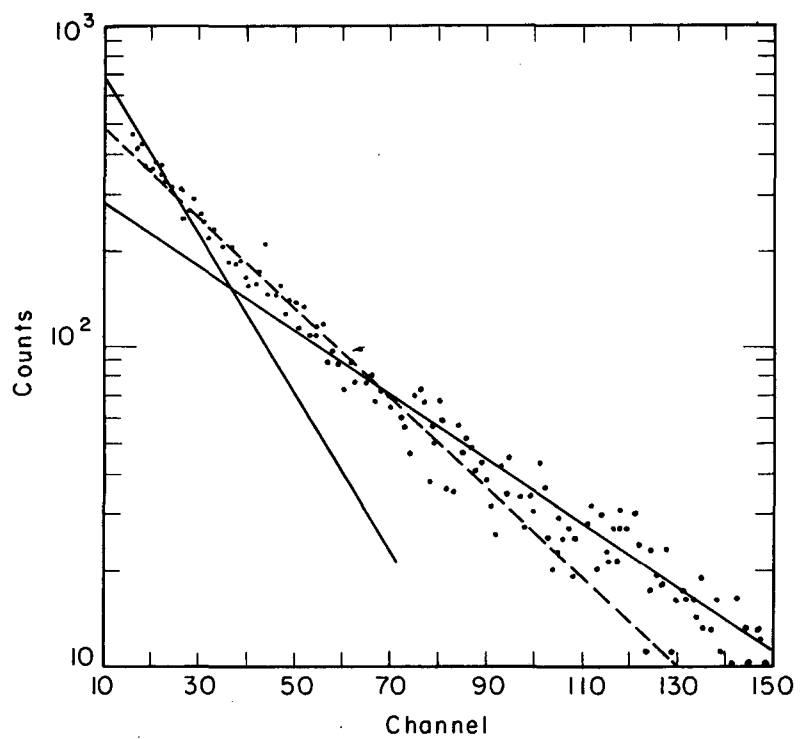
MU-33583

Fig. 14. Graph of counts versus time for all alpha particles detected at an incident-particle energy of 22.5 MeV. Channel address time is 0.01 sec.
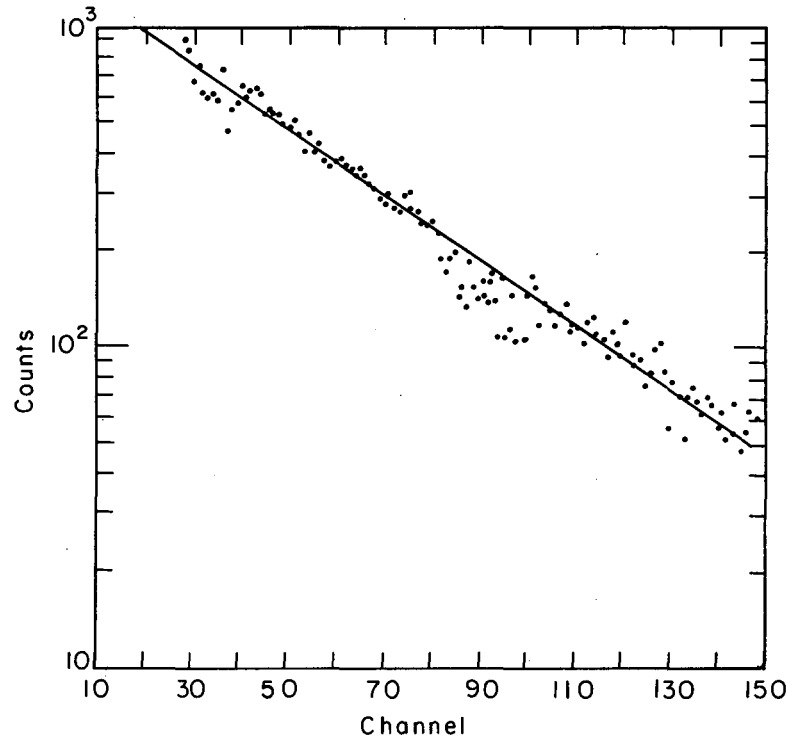
MU-33584

Fig. 15. Counts versus time for 7.60- and 7.66-MeV alpha
particles at an incident-particle energy of 22.5 MeV.
Channel address time is 0.01 sec.
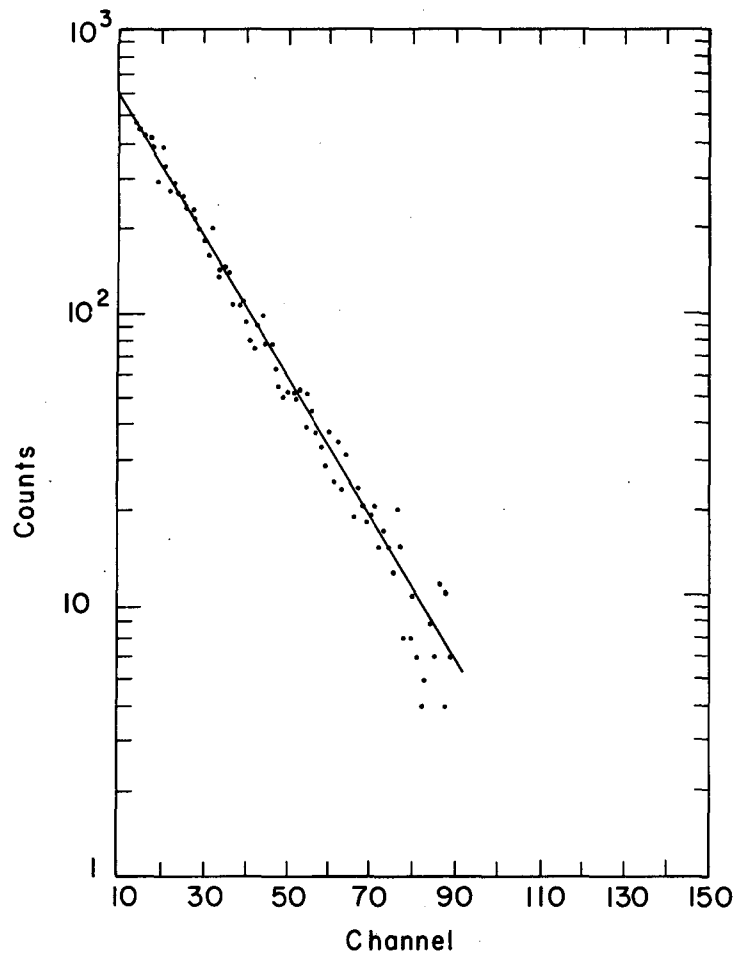
Fig. 16. Counts versus time for 7.82- and 7.88-MeV alpha
    particles at an incident-particle energy of 22.5 MeV.
    Channel address time is 0.01 sec.
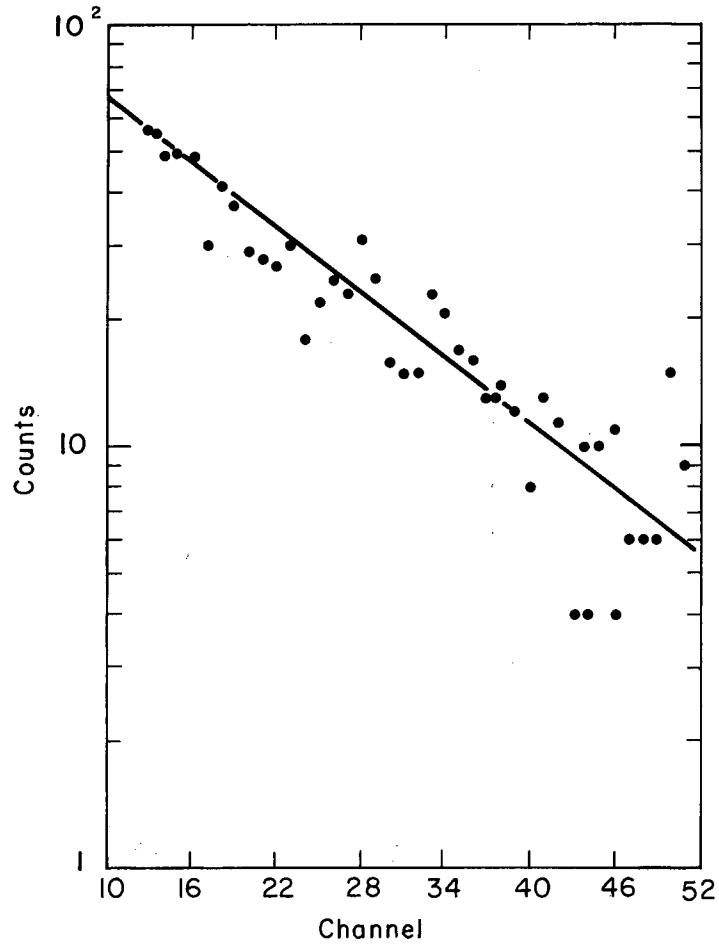
Fig. 17. Counts versus time for 7.60-MeV alpha particles at an incident-particle energy of 22.5 MeV. Channel address time is 0.01 sec.

Inasmuch as we have

$$s = \frac{\int_0^{n\Delta t} t \, dN}{\int_0^{n\Delta t} dN} = \tau \left[1 - \frac{\frac{n\Delta t}{\tau}}{\exp(- n\Delta t/\tau) - 1} \right]$$

successive approximations of τ, the true mean life, can be obtained. Peierls has shown that for $\Delta t \leq 0.1 \, \tau$, the error introduced by finite time intervals of counting is less than 0.2%. This method can also be used for determining the standard error of the mean life in the limiting case where the background is negligible. Then we have $\sigma = \tau/\sqrt{N}$. For our case, Evans[56] presents a graph based on Peierls' method and verified by Fisher's "method of maximum likelihood." This graph was used to obtain the standard error (see Table IV). A comparative tabulation of the data with half lives determined by this method follows:

Alpha energy (MeV)	Half life (sec)
7.60 + 7.66	$0.301 \pm .007$
7.60	$0.292 \pm .018$
7.82 + 7.88	$0.119 \pm .003$ and $0.123 \pm .003$
7.88	$0.124 \pm .018$

These data were analyzed using a computer program which gives an iterative least-squares fit,[57] including the standard deviations in a_j and λ_j of the function

$$A_t = \sum_{j=1}^{2} a_j e^{-\lambda_j t} \quad ,$$

where t is the elapsed time, a_j is the activity of each component at $T = 0$, and λ_j is the decay constant of component j. Naturally, this program was most effective in separating the two components in Run 1 (where all alpha groups contributed to the half-life data). The half life of component 1 is $0.131 \pm .02$ sec, and that of component 2 is $0.329 \pm .04$ sec.

Table IV. Calculation of half lives by the method of Peierls.[a]

Channels	$T_o = n\Delta t$ (sec)	s^b (sec)	T_o/s	τ/s	τ (sec)	$T_{1/2}$ (sec)	$\sigma(\sqrt{N}/\tau)$	$\sqrt{N}$	σ
Run 1[c,d]									
16-28	0.12	0.0590	2.04	>2	>0.12	>0.083	>6	68	>0.011
16-37	0.21	0.088	2.39	~2.0	~0.176	~0.122	4.6	84.4	0.0096
16-51	0.35	0.1345	2.60	1.72	0.231	0.160	4.2	96.5	0.0105
16-66	0.50	0.174	2.87	1.49	0.259	0.1795	3.6	103.5	0.009
16-80	0.64	0.2045	3.13	1.32	0.270	0.187	3.1	108	0.0078
16-95	0.79	0.2315	3.41	1.22	0.282	0.195	2.4	110.8	0.0061
16-110	0.94	0.2525	3.72	1.15	0.290	0.201	2.4	112.6	0.0054
16-124	1.08	0.272	3.97	1.115	0.303	0.210	1.75	114	0.0047
Run 2[c,e]									
28-37	0.09	0.0459	<2	>>2.0	>>0.09	>>0.06	>>6	82.4	>>0.0066
28-59	0.31	0.142	2.18	>2	>0.284	>0.197	>5	134.1	>0.0106
28-66	0.38	0.1685	2.25	~2.0	~0.337	~0.2335	~5	143.1	~0.0118
28-81	0.53	0.2175	2.44	~1.9	~0.412	~0.286	4.5	143.2	~0.0118
28-95	0.67	0.250	2.68	1.65	0.413	0.286	4.0	157	0.0100
28-116	0.88	0.2905	2.97	1.42	0.421	0.292	3.4	164.3	0.0088
28-124	0.96	0.315	3.05	1.38	0.434	0.3008	3.3	172	0.0083
28-138	1.10	0.3395	3.24	1.28	0.435	0.3013	2.85	174	0.007
28-153	1.25	0.3615	3.47	1.19	0.431	0.2988	2.5	179.4	0.006
Run 3[c,f]									
14-25	0.0534		<2.0	>2.0	>0.107	>0.074	>6	65.6	>0.0096
14-37	0.0925		2.49	~1.9	~0.176	~0.122	4.4	80.1	0.0097
14-53	0.126		3.10	1.35	0.170	0.118	3.15	87.3	0.0062
14-66	0.144		3.61	1.18	0.170	0.118	2.3	89.6	0.0044
14-78	0.155		4.13	1.10	0.171	0.119	1.6	90.9	0.003
Run 4[c,g]									
13-23	0.10	0.0474	2.11	>2	>0.0948	>0.066	>5.5	21.9	0.024
13-33	0.20	0.0837	2.39	~1.9	~0.159	~0.110	~4.6	24.8	0.030
13-44	0.31	0.1122	2.76	1.68	0.188	0.130	3.9	27.2	0.027
13-52	0.39	0.1310	2.98	1.41	0.185	0.128	3.4	28.3	0.022
13-60	0.47	0.1428	3.29	1.26	0.180	0.124	2.8	28.8	0.018

a. See reference 56.

b. $s = \dfrac{\sum\limits_{i}(2i-1)\Delta N_i}{\sum \Delta N_i}$

c. $\Delta t = 0.01$ sec.

d. All alpha particles detected.

e. Alpha energies are 7.60 and 7.66 MeV.

f. Alpha energies are 7.82 and 7.88 MeV.

g. Alpha energy is 7.88 MeV.

When analyzed singly with the above program, the separated alpha groups gave the following results:

| Alpha energy (MeV)	Half life (sec)
7.60 + 7.66	0.295±.005
7.60	0.274±.010
7.82 + 7.88	0.117±.002 and 0.124±.004
7.88	0.124±.009

These results are consistent within experimental error. The 7.60-MeV group has the same half life as the 7.60- + 7.66-MeV groups (the 7.66-MeV group was produced in more than four times that of the 7.60-MeV group, and the 7.88-MeV group was produced in more than three times that of the 7.82-MeV group, so it was assumed that the half life for the 7.88-MeV group is within experimental error equal to that of the summed 7.82- + + 7.88-MeV group).

C. Excitation-Function and Cross-Section Determination

The absolute excitation functions were determined by using the same geometry for the measurement of the production of the unknown (At^{212}) (both isomeric states) and for the formation of At^{211} as a function of the energy of alpha particles. The excitation functions for the $Bi^{209}(\alpha,2n)At^{211}$ have been accurately measured[1] and verified.[2]

The excitation functions for the separate isomeric states of At^{212} were first determined at the 60-Inch Cyclotron and redetermined at the 88-Inch Cyclotron. The initial determinations (with the mechanically controlled equipment) were made to obtain the thresholds, maxima, and shapes of the two curves. Results of the experiments at the 88-Inch Cyclotron are shown in Fig. 18 and tabulated in Table V.

The yield of recoiling nuclei from the (α,n) and the $(\alpha,2n)$ reactions was controlled by having the target thickness less than 20 $\mu g/cm^2$, so the energy loss of the recoiling nuclei in traversing the target thickness could be neglected. The recoiling nuclei have a range from 60 to 100 $\mu g/cm^2$ in bismuth.[58] The energy of the recoiling nucleus, E_r, equals the sum of the kinetic energy of the incoming helium ion, E_α, and the Q of the
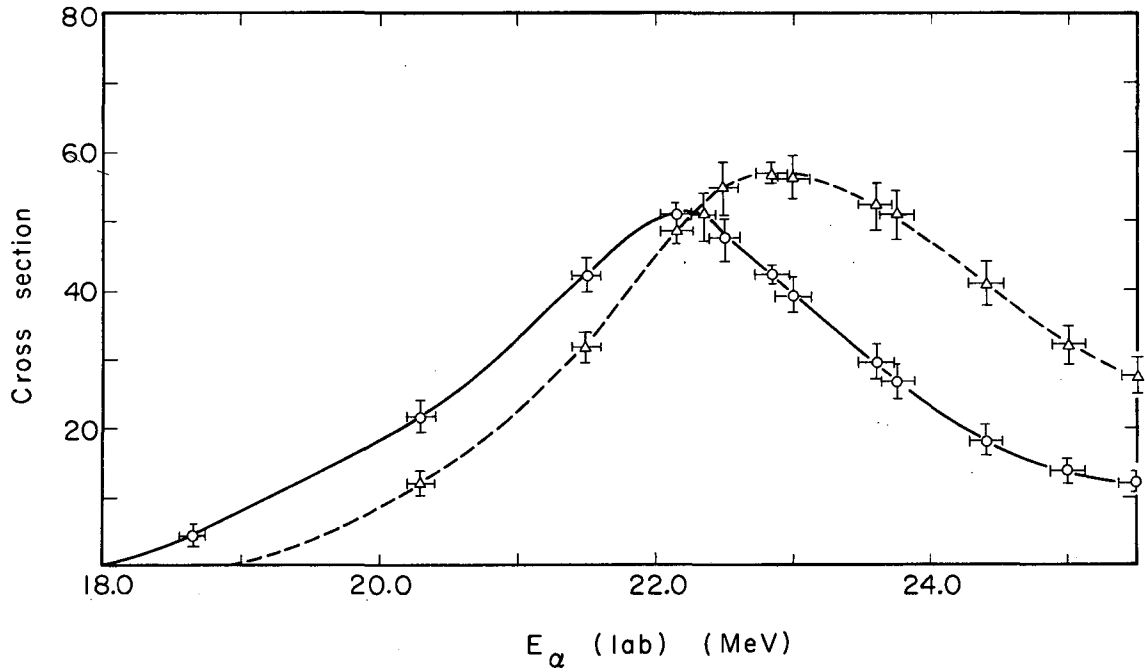
Fig. 18. Absolute cross section for production of 7.60- and
7.66-MeV alpha emitter (solid curve) and of 7.82- and
7.88-MeV alpha emitter (dashed curve) for incident alpha-
particle energies from 18 to 25.5 MeV.

Table V. Data collected at the 88-Inch Cyclotron for cross-section determinations. All runs are 1/2 hour except for foils A-10 and A-11, which are 2.2 and 1.4 hours, respectively.

Foil	Energy (MeV)	Integrated beam current (μA-h)	Alpha counts					Counts/μA-h		σ (mb)	
			7.60 + 7.66 MeV	7.60 MeV	7.82 + 7.88 MeV	7.88 MeV	7.43 MeV	7.60 + 7.66 MeV	7.82 + 7.88 MeV	7.60 + 7.66 MeV	7.82 + 7.88 MeV
B-11	18.65	0.0014	11					8000		4.7±1.4	
B-4	23.0	0.0036	239	47	343	103	~2 to 4	66390	95280	39.3±2.5	56.4±3.0
B-6	21.5	0.0040	285	39	215	78		71250	53750	42.1±2.5	31.8±2.2
B-0	25.0	0.0025	58	14	135	51	19	23200	54000	13.7±1.8	32.0±2.8
B-5	22.35	0.0025	214	45	214	72	53	85600	85600	50.7±3.5	50.7±3.5
B-9	20.3	0.0025	92	14	51	19	56	36800	·20400	21.8±2.3	12.1±1.7
A-6	25.5	0.0025	50	11	116	51	91	20000	46400	11.8±1.7	27.4±2.5
A-10	23.6	0.0025	125	29	220	65	80	50000	88000	29.6±2.6	52.1±3.5
A-9	24.4	0.0025	76	20	172	71	149	30400	68800	18.0±2.1	40.7±3.1
A-9	23.75[a]	0.0025	113	19	215	71	175	45200	86000	26.8±2.5	50.9±3.5
A-11	22.15	0.0025	212	34	188	55	147	84800	77200	50.1±3.4	45.6±3.3
B-3	22.5	0.0025	209	34	233	65	195	80360	92800	47.5±3.3	54.9±3.6
A-10	22.85	0.0154	1095	230	1482	433	849	71400	96230	42.2±1.3	57.0±1.5
A-11	22.15	0.0113	971	160	930	285	741	85950	82300	50.9±1.6	48.5±1.6
Background							165				
0-0	31.3	0.100[b]						53721			
c								16435			

a. Cyclotron parameters changed to reduce energy by ~0.6 MeV.

b. Cyclotron operated continuous-wave (nonpulsed); therefore the beam increased by a factor >10. The foil was counted for 550.7 min after bombardment.

c. Foil counted for 385.0 min.

reaction less the kinetic energy of the neutron, E_n. For our case, E_n is approximately 2.5 MeV;[59] thus, since Q equals 14 MeV, we have

$$E_r = E_\alpha - 16.5 \ .$$

Similarly, $E_r(\alpha, 2n)$ is

$$E_r = E_\alpha - 24.3 \ .$$

Comparing the cross section of the (α, n) reaction at 23.5 MeV to the $(\alpha, 2n)$ reaction at 31.5 MeV, one should find equal probability of the recoiling nuclei's escaping from the target.

The maximum angle of scattering, θ_{max}, of the recoil nucleus is calculated from the kinematical relationship

$$\sin \theta_{At} = \frac{E_n M_n}{E_{At} M_{At}} \sin \theta_n \ ,$$

where n means neutron. It has been determined that the average kinetic energy for the neutron is 2.5 MeV.[59] Assuming

$$P(T) dt = \frac{T}{\tau^2} e^{-T/\tau} dT \ ,$$

where $P(T)$ is the probability of emission at an energy T, and τ is the nuclear temperature (assumed to be 1.2 MeV), one calculates that 99% of the neutrons are emitted with energies less than

$$T = 7\tau \quad \text{or} \quad T = 8.4 \text{ MeV} \ .$$

Thus, if one assumes the maximum neutron energy to be 8.5 MeV, then 99% of the recoiling nuclei are included. If we further assume $(\sin \theta_n)_{max} = 1$, that is $\theta_n = \pi/2$, then $(\theta_{At})_{max}$ is 12 deg for an E_α of 23.5 MeV. This statistical relation breaks down when the residual nucleus is at an excitation energy less than 4 MeV. However, this means only that the transitions are to discrete states at lower energies.[60] The work of Donovan, Harvey, and Wade verifies that the $(\alpha, 2n)$ angular distribution of the recoiling nuclei and recoil range are very comparable to the $(\alpha, 3n)$ distribution and by extension should be similar to the (α, n) results.[3]

No quantitative attempt was made to determine the excitation functions of the 7.60-MeV and the 7.88-MeV groups, as their yields were so low as to preclude adequate statistics. In general, they appear to be produced in constant ratios relative to the total production of their particular state, independent of the energy of the incoming alpha particle (see Table VI). The ratio of the 7.60-MeV group to the 7.60- + 7.66-MeV group is 18.7% and the ratio of the 7.88-MeV group to the 7.82- + 7.88-MeV group is 30.5%.

The ratio of the cross section for the production of the high spin state to that for the low spin state $(\sigma_m/\sigma_{g.s.})$ is tabulated in Table VII (see also Fig. 19).

Measurement of the relative cross sections is dependent upon the modes of decay of the members being investigated. Thus, it was necessary to study the decay modes of the astatine isomers and to verify that the isomeric state did not feed the ground state.

De-excitation by gamma decay, as described in the section on HiLAC experiments, was investigated by searching for the conversion electrons. This was a sensitive method of searching for low-energy transitions, since the conversion efficiency should be high (see Table VIII for calculations of these conversion factors). De-excitation of At^{212} by γ-rays of energy from 120 to 700 keV was not greater than 1-mb cross section at incident alpha particle energy of 23 MeV and therefore could not have occurred in more than 2% of the cases.

A 60-keV gamma ray appears to have a half life of 0.13 sec.[55] This could be explained by alpha transitions from each At^{212} state to each of two levels of Bi^{208}, 60-keV apart,[61] as shown in Fig. 20. The calculations given in Table IX[62] indicate that the 220-keV γ-de-excitation of At^{212m} must be slower than that corresponding to an M3 transition. Thus, there must be a difference of at least three $\hbar$ angular-momentum units between the isomers of At^{212}.

Table VI. Ratios of 7.60/(7.60 + 7.66) MeV and 7.88/(7.82 + 7.88) MeV
cross sections for incident-particle energies from 20.3 to 25.5 MeV.

Energy (MeV)	Counts 7.60 MeV	Counts 7.60 + 7.66 MeV	7.60 MeV total	R.m.s. deviation	Counts 7.88 MeV	Counts 7.88 + 7.82 MeV	7.88 MeV total	R.m.s. deviation
20.3	14	92	0.15	±.04	19	51	0.37	±.09
21.5	39	285	0.14	±.02	78	215	0.36	±.04
22.15	34	212	0.16	±.03	55	188	0.29	±.04
22.15	160	971	0.16	±.01	285	930	0.31	±.02
22.35	45	214	0.21	±.03	72	214	0.34	±.04
22.5	34	209	0.16	±.03	65	233	0.28	±.03
22.85	230	1095	0.21	±.01	433	1482	0.30	±.01
23.0	47	239	0.20	±.03	103	343	0.30	±.03
23.6	29	125	0.23	±.04	65	220	0.30	±.04
23.75	19	113	0.17	±.04	71	215	0.33	±.04
24.4	20	76	0.26	±.04	71	172	0.41	±.05
25.0	14	58	0.24	±.06	51	135	0.38	±.05
25.5	11	50	0.22	±.07	51	116	0.44	±.06
Average			0.185±.01				0.30±.01	

Table VII. Ratios of cross sections
for (7.82 + 7.88)/(7.60 + 7.66)-MeV alpha emitters
for incident-particle energies from 20.3 to 25.5 MeV.

Lab. alpha energy[a] (MeV)	$\sigma_{g.s.}$[b] (mb)	σ_m[c] (mb)	$\sigma_m/\sigma_{g.s.}$
18.65	4.7±1.4	<1.0	
20.3	21.8±2.3	12.1±1.7	0.55±.1
21.5	42.1±2.5	31.8±2.2	0.76±.07
22.15	50.1±3.4	45.6±3.3	0.91±.09
22.15	50.9±1.6	48.5±1.6	0.95±.04
22.35	50.7±3.5	50.7±3.5	1.00±.10
22.5	47.5±3.3	54.9±3.6	1.15±.11
22.85	42.2±1.3	57.0±1.5	1.35±.05
23.0	39.3±2.5	56.4±3.0	1.43±.12
23.6	29.6±2.6	52.1±3.5	1.76±.19
23.75	26.8±2.5	50.9±3.5	1.90±.22
24.4	18.0±2.1	40.7±3.1	2.26±.30
25.0	13.7±1.8	32.0±2.8	2.33±.37
25.5	11.8±1.7	27.4±2.5	2.32±.39

a. Energy of alpha particles from the cyclotron assumed to be
33 MeV. The beam was degraded through Al foils which were
weighed to ±0.5%.[46]

b. 7.60 + 7.66 MeV; $T_{1/2}$ = 0.30 sec.

c. 7.82 + 7.88 MeV; $T_{1/2}$ = 0.12 sec.
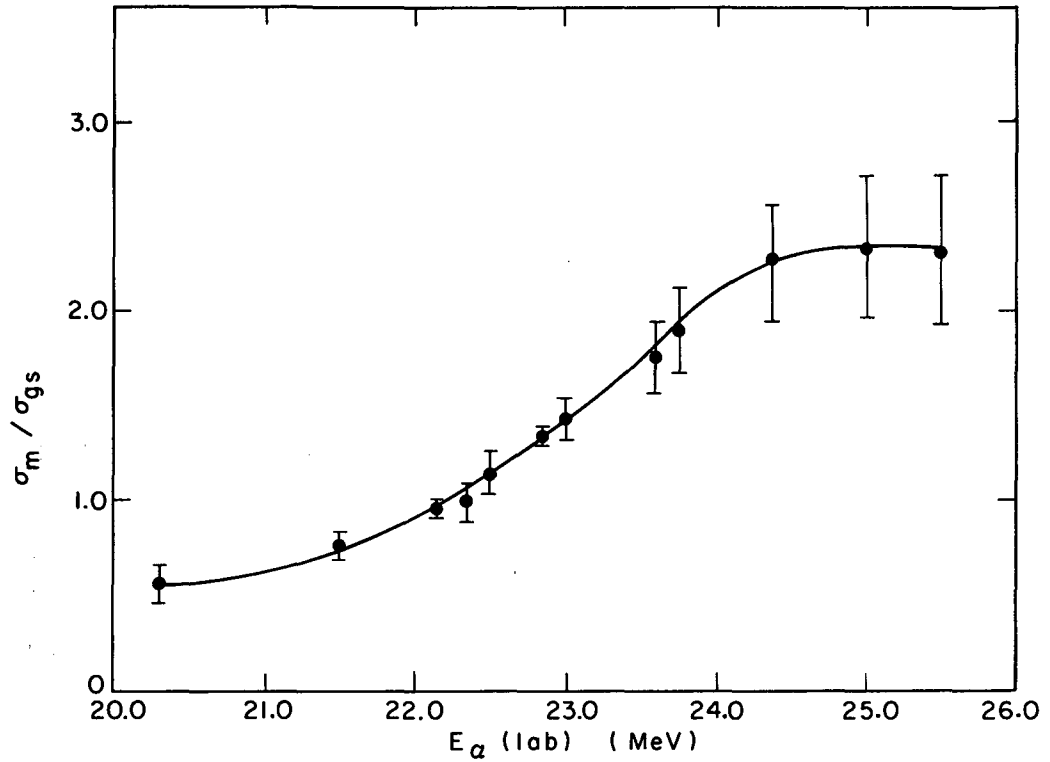
MU-33588

Fig. 19. Ratio of cross sections for production of 7.82- and
7.88-MeV to 7.60- and 7.66-MeV alpha emitters (designated
as σ_m/σ_{gs}. for incident alpha-particle energies of 20.3 to
25.5 MeV.

Table VIII. Calculations of conversion-electron production efficiencies for gamma-emission energies of 60, 220, and 511 keV for Z = 83 and 85.

Transition	K	L_I	L_{II}	L_{III}	M_I	M_{II}	M_{III}	M_{IV}	M_V	K/L/M	Ne/Nq
				E = 60 keV, Z = 83, k = 60/511 = 0.117							
E1		0.124	0.087	0.110	0.047	0.031	0.038	0.006	0.007	0/1.0/0.4	0.45
M1		7.0	0.671	0.063	3.51	0.378	0.025	0.005	0.002	0/1.0/0.51	11.7
E2		1.0	42.0	41.6	0.60	18.9	19.3	0.39	0.28	0/1.0/0.32	122.5
M2		238.0	20.2	98.0	104.0	9.8	49.8	0.6	0.07	0/1.0/0.46	520.5
				E = 220 keV, Z = 85, k = 220/511 = 0.43							
E3	0.356	0.176	1.77	0.76	0.08	0.08	0.04	0.01	0.01	1.0/7.6/2.6	4.01
M3	13.3	6.3	1.1	3.5	2.6	0.54	1.9	0.04	0.02	1.0/0.37/0.17	29.3
E4	Too long-lived										
				E = 511 keV, Z = 83, k = 511/511 = 1.0							
E1	0.008	0.001	0.0001	0.0001	0.0003					1/0.15/0.04	~0.01
M1	0.096	0.014	0.001	0.0001	0.007	0.0008				1/0.16/0.08	~0.11
E2	0.021	0.003	0.003	0.001	0.001	0.0001				1/0.33/0.05	0.03
M2	0.26	0.05	0.007	0.002	0.018	0.003	0.001			1/0.23/0.08	0.33
E3	0.052	0.01	0.02	0.005	0.004	0.009	0.002			1/0.67/0.29	0.10
M3	0.58	0.14	0.03	0.02	0.06	0.001	0.001			1/0.33/0.10	0.83
E4	0.024	0.036	0.10	0.02	0.014	0.044	0.009	0.001		1/6.5/2.8	0.25
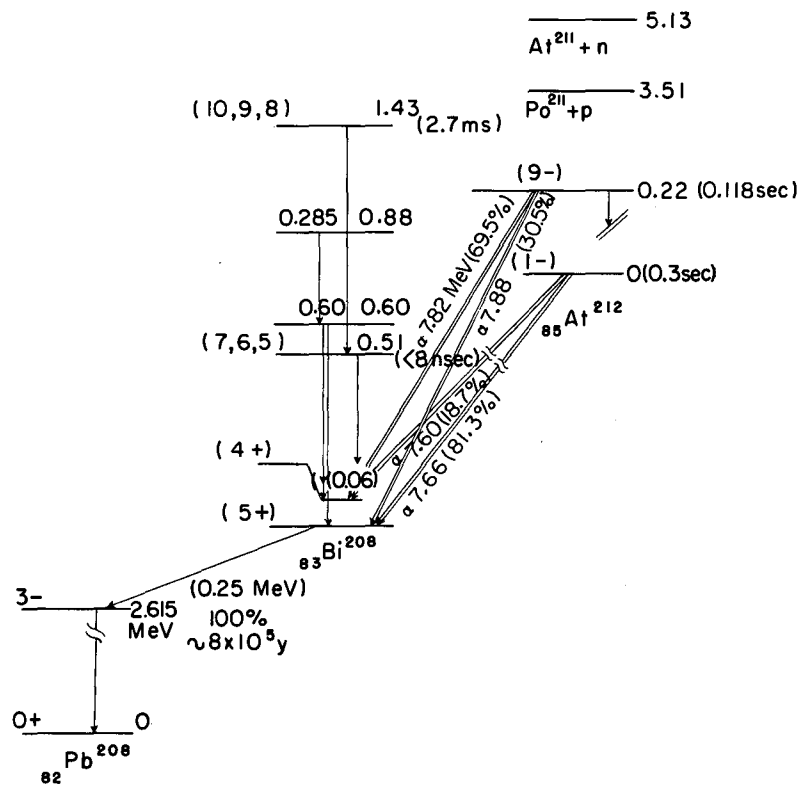
Fig. 20. Proposed decay scheme for At^{212}.

MU-33571

Table IX. De-excitation transition probabilities
for gamma energies of 220 and 60 keV
with A = 212 and 208, respectively.

Multi-polarity	T_{SP}	$T_{1/2}$ (sec) [a]
	For A = 212 and E_γ = 220 keV	
E1	$1.5 \times 10^{14} A^{2/3} E_\gamma^3 = 0.571 \times 10^{14}$	1.21×10^{-14}
M1	$2.8 \times 10^{13} E_\gamma^3 = 0.3 \times 10^{12}$	2.31×10^{-12}
E2	$1.6 \times 10^8 A^{4/3} E_\gamma^5 = 0.104 \times 10^9$	6.66×10^{-9}
M2	$1.2 \times 10^8 A^{2/3} E_\gamma^5 = 0.22 \times 10^7$	3.14×10^{-7}
E3	$1.1 \times 10^2 A^2 E_\gamma^7 = 0.124 \times 10^3$	5.59×10^{-3}
M3	$1.8 \times 10^2 A^{4/3} E_\gamma^7 = 0.566 \times 10^1$	1.22×10^{-1}
E4	$5 \times 10^{-5} A^{8/3} E_\gamma^9 = 0.0962 \times 10^{-3}$	7.2×10^3
	For A = 208 and E_γ = 60 keV	
E1	$1.5 \times 10^{14} A^{2/3} E_\gamma^3 = 0.114 \times 10^{13}$	6.07×10^{-12}
M1	$2.8 \times 10^{13} E_\gamma^3 = 0.605 \times 10^{10}$	1.14×10^{-10}
E2	$1.6 \times 10^8 A^{4/3} E_\gamma^5 = 0.156 \times 10^6$	4.44×10^{-6}
M2	$1.2 \times 10^8 A^{2/3} E_\gamma^5 = 0.328 \times 10^4$	2.11×10^{-4}
E3	$1.1 \times 10^2 A^2 E_\gamma^7 = 0.135 \times 10^{-1}$	5.14×10

a. Here we have $T_{1/2} = 0.693/T_{SP}$.

D. Summary of Experimental Results

When bismuth was bombarded by doubly charged helium ions whose kinetic energy was between 16 and 26 MeV, the following results were obtained:

1. Two products were observed: $_{83}Bi^{209}(\alpha,n)_{85}At^{212}$

   and $_{83}Bi^{209}(\alpha,n)_{85}At^{212m}$.

2. The relative yield of these products was found:

Reaction	Observable threshold (greater than 1 mb)	Maximum cross section (mb)
$Bi^{209}(\alpha,n)At^{212}$	18 MeV	51 at 22.2 MeV
$Bi^{209}(\alpha,n)At^{212m}$	18.7 MeV	57 at 22.8 MeV

3. Decay characteristics are:
   a. $At^{212} \rightarrow Bi^{208} + \alpha$ with a half life of $T_{1/2} = 0.30$ sec.

   $$\alpha \text{ energy} = \begin{matrix} 7.66 \text{ MeV } (81.3\%) \\ 7.60 \text{ MeV } (18.7\%) \end{matrix} .$$

   b. $At^{212m} \rightarrow Bi^{208} + \alpha$ with a half life of $T_{1/2} = 0.118$ sec.

   $$\alpha \text{ energy} = \begin{matrix} 7.82 \text{ MeV } (69.5\%) \\ 7.88 \text{ MeV } (30.5\%) \end{matrix} .$$

Conclusions drawn from experimental results are shown in Fig. 20.

IV. DISCUSSION

A. Mass Assignments

The Bi(α,n)At reaction was identified as the investigated reaction at bombardment energies of 16 to 25 MeV. Table X shows excitation functions for reactions induced by alpha particles incident upon Bi, which have been determined by various experimenters.[1-3,11,63,64] From Table X it is apparent that the alternate products have been investigated and identified. Similarly, the Q's for the various reactions have been calculated, and only the α,n reaction has a threshold that permits an appreciable yield at 19-MeV incident alpha-particle energy. The various alternate products have been investigated, decay schemes set up, and half lives measured for these products. All these factors indicate that an alternate reaction is not probable.

B. Decay Energy

The alpha-decay energies were determined and verified several times. The energies agree closely with the results of Ritter and Smith,[8] if we consider that, being unable to resolve the alpha groups, they collected them together and thus obtained an average decay energy. Their figure of 7.87 MeV for the decay energy is consistent with this average.

C. Half Lives

In contradiction to previously reported results, the half lives obtained here demonstrate that there is no half life of 0.2 sec; thus, this value must be an average half life for two or more components. Analysis of the data, using the "Frenic" code[57] on the 7090 computer, bears out this conclusion. The total data could be fitted to a single slope or to two slopes, and only by taking data during a much longer period would the true case be established. This problem was obviated by determining independently the half lives of the separate alpha groups. The various figures showing the decay of the individual alpha groups substantiate assignments of separate half lives to these groups. The

Table X. Characteristics of the bombardment of Bi^{209} with alpha particle of 40 MeV or less.

Reaction	Product[a]			Max. σ (barns)	$E_{max. σ}$ (MeV)	$E_{thresh.}$ (MeV)
	Decay	Energy (MeV)	$T_{1/2}$			
$Bi^{209}(\alpha,\gamma)At^{213}$	α	9.2	2 sec	0.001^{b}	---	---
$Bi^{209}(\alpha,2n)At^{211}$	α(40%) K(60%)	5.86 0.78	7.2 h	0.91^{b}	31.5	22
$Bi^{209}(\alpha,3n)At^{210}$	α(0.05%) K(~100%)	5.36 1.0	8.3 h	1.5^{c}	40^{d}	26
$Bi^{209}(\alpha,p)Po^{212}$	α α	8.78 11.65	0.3 sec 46 sec	0.004^{e}	39^{c}	---
$Bi^{209}(\alpha,pn)Po^{211}$	α α	7.44 7.14	0.5 sec 25 sec	$0.008^{e,f}$	40^{e}	39

a. D. Strominger et al., reference 65.

b. E. L. Kelly et al., reference 1.

c. W. J. Ramler et al., reference 2.

d. W. John, Jr., reference 11.

e. F. N. Spiess, reference 64.

f. D. H. Templeton et al., reference 63.

existence of only two half lives can be explained by the assumption that there are two states of At^{212} decaying to two states of Bi^{208}. This assumption can be made because the cross section of γ de-excitation of astatine is less than 1 mb when a thick bismuth target is irradiated with 23-MeV alphas. However, as previously reported, a 60-keV γ-ray with L/M spacing characteristic of bismuth was observed with a half life of 0.130 sec and a cross section of approximately 100 mb.[55] The proposed decay scheme substantially conforms to the above data. If coincidence experiments were performed, then the gammas could be associated with their own specific α decay, but this would require extensive investigation.

D. Decay Schemes

The proposed decay scheme for At^{212} (Fig. 20) shows the decay of isomeric states to Bi^{208}. The decay of At^{212} to Po^{212} was not observed (either β^{+} or K capture). However, this would appear to be too long lived to be a competitive mode of decay, as the decay energy should be 1.83 MeV (see Fig. 21). If one uses the equation[66]

$$\log f_{\beta^{+}} = 4.0 \log E_{0} + 0.80 - 0.007\ Z - 0.009\ Z(\log \frac{E_{0}}{3})^{2} ,$$

then even for super-allowed β transitions for which $\log(ft)$ would be 3, the half life would be 1 min, so no β^{+} or K capture would be observed. In the present case it is assumed that the decay is from 1- to 0+ levels, so it would be the first forbidden decay[67] for which $\log(ft)$ ought to be equal to or greater than 6. Therefore the K-capture half life is greater than 10^{6} alpha half lives, so the K-capture decay mode can be neglected.

The closed cycle for the 4n series (see Fig. 22) shows that decay energy from the ground state At^{212} to the ground state Bi^{208} should be approximately 8 MeV.[30,32] Thus, the alpha transition to the 1.43-MeV excited state would not be observed, because there is so little energy available (the 1.43-MeV state has a half life of 2.7 msec[61]). The other states (below the 1.43-MeV level) would be de-excited by γ emission in
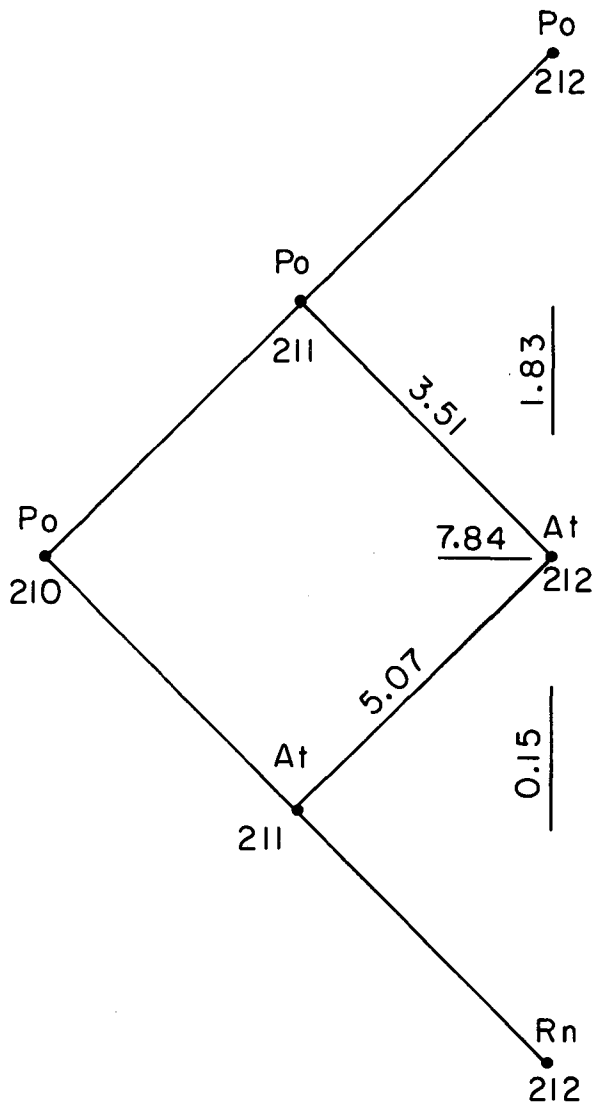
Fig. 21. Proposed mass-difference chart for masses of 210, 211, and 212 and atomic numbers of 84, 85, and 86.
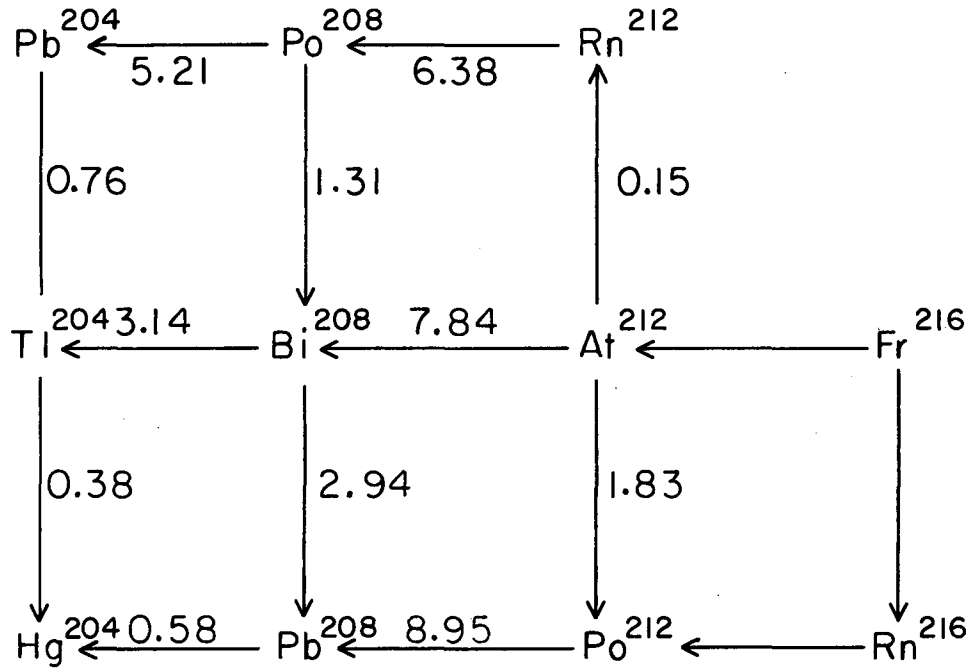
Fig. 22. Chart of closed cycle for 4n series between lead
and radon for masses 204 through 216.

the 100-to 800-keV region, so they would have been observed in the conversion-electron detection experiments. This reasoning is justified, since the table of conversion coefficients (Table VIII) demonstrates that an appreciable portion of the γ emission would appear as conversion electrons.

E. Spin Assignments

The choice of 1- and 9- for the states of At^{212} and At^{212m}, respectively, can not be clearly demonstrated experimentally. The 1- state has been selected as the ground state because Nordheim's rule[25,68] stipulates that if $j_1 + j_2 + \ell_1 + \ell_2$ is an even number, where the j's and ℓ's represent spin andorbital angular momentum of the respective particles, then J equals $|j_1 - j_2$, where J is the total spin (the strong rule). Thus, as in this case, j_1 is 9/2; ℓ_1 is 5; j_2 is 9/2; ℓ_2 is 4; then J is $|j_1 - j_2|$ which should lead to $J = 0$ as the ground state. However, the ground state appears to be 1-, similar to that of Bi^{210} as discussed by Kim and Rasmussen.[28] The ground state cannot be $J = 0$, because there is an alpha decay to the two lowest levels of Bi^{208}. Because these are well established as 5+ and 4+,[69] it can be stated definitely that this alpha decay does not originate from a $J = 0$ state.[70] That $J = 1$ is a clear violation of the Nordheim strong rule as modified by Brennan and Bernstein. A possible explanation is that the ground state of At^{212} was never reached. That is, the alpha decay is from two excited isomeric states of At^{212}. This means that there are two states of different angular momenta with an energy separation of only 220 keV and still separate from the ground state. The lower state must lie within 0.5 MeV of that ground state. The alpha decaying states cannot differ by less than 4 $\hbar$ of angular momentum or they could de-excite through γ emission. The maximum J cannot be greater than nine if single-particle states within the shell model are assumed. This would require that the energy levels would be high for $J = 1, 2, 3, 4$ or 5, 6, 7, and 8, and low for 0, 4 or 5, and 9, which does not appear to be probable in the light of the theoretical calculations in this region.[27] A second

alternative is that the 4 and 5 states of Bi^{208} have opposite parity. However, all calculations on this nucleus,[28,71,72] and experimental results[69] indicated that these states are of the same parity.

Thus, a 1- spin must be assigned to the ground state of At^{212} to be consistent with the experimental data for Bi^{208} and Bi^{210}. This is not the first contradiction of the modified Nordheim strong-coupling rule; Bi^{210} is also an example.[69] Kim,[28] using a tensor force, has given strong theoretical arguments for the breakdown of the modified Nordheim strong-coupling rule. These arguments should hold for At^{212} also, because the shell-model configurations are quite similar.

F. Decay Characteristics

The empirical decay-hindrance factor, defined by Gallagher and Rasmussen,[42] can be justified from the WKB barrier-penetration formulae. A very significant calculation is the relative hindrance of the various decay groups within one isotope. In this instance, the barrier is equivalent; the only variables are the radial wave functions and the angular momentum. The hindrance factor F is defined by Gallagher and Rasmussen as

$$\log_{10} F = \log_{10} T_{1/2} - A_z Q_{eff}^{-1/2} - B_z \quad .$$

Here the decay energy is

$$Q_{eff} = E_\alpha + E_R + \Delta E_{sc}$$

where E_α is the kinetic energy of the particle, E_R is the recoil energy of the residual nucleus,

$$E_R = \frac{M_\alpha}{M_R} E_\alpha \quad ,$$

and ΔE_{sc}, the electron screening energy, is

$$\Delta E_{sc} = 65.3 \; z^{7/5} - 80 \; z^{2/5} \quad .$$

Thus we can write

$$Q_{eff} = \frac{M_\alpha + M_R}{M_R} E_\alpha + 65.3 - (\frac{80}{z+2})^{7/5} .$$

In the equation of Gallagher and Rasmussen, A_z and B_z are constants for the particular element measured; $A_{85} = 133.40$ and $B_{85} = -51.1913$ are the interpolated values of A_z and B_z for $z = 85$.[73] Table XI gives the value for the hindrance factor for the four alpha decay groups of At^{212}. These decays are a good subject of investigation, inasmuch as the ratio of hindrance factors should be dependent upon the angular momentum transferred and the vector coupling coefficients. For this particular case, the radial wave function is the same for all decay modes (all the protons are in the $h_{9/2}$ shell, and the neutrons are in the $g_{9/2}$ and $p_{1/2}$ shells). In this paper the investigation is limited to first-order approximations only. The theoretical approach of Mang and Zeh,[38] using configuration mixing and fractional parentage, leads to a more quantitative result. The essential feature is that decays from the 1- to 4+ and the 9- to the 5+ states are hindered more than the ground-to-ground (1- to 5+) and excited-to-excited (9- to 4+) decays. It is proposed that the more hindered cases have the same mechanism, and similarly the 1- to 5+ and 9- to 4+ also have the same mechanism. The difference between these two sets of decay is that a "spin flip" is required for the more hindered decays. It is assumed that the five units of angular momentum are transferred for all of these cases.

G. Alpha-Energy Schematics and Decay-Energy Cycles

The method of plotting the mass number against alpha energy (Fig. 23) demonstrates how accurately the decay energy can be predicted. The alpha-decay energy of At^{212} is quite difficult to estimate because it is in a region of very rapidly varying energy as a function of mass. However, the predicted decay energy is within 40 keV of the measured value. The sudden break in decay energy with mass is due to crossing the closed neutron shell of $n = 126$. It is readily seen that this same discontinuity is present for all z.

Table XI. Hindrance factors for the decay of $_{85}At^{212}$

Alpha kinetic energy (MeV)	$Q_{eff.}$ (MeV)[a]	Decay (%)	$T_{1/2}$ (sec)	Log_{10} partial $T_{1/2}$	Log_{10} F	F
7.60	7.78	0.187	0.300	0.2053	3.5666	3687
7.66	7.84	0.813	0.300	9.5670-10	3.2183	1310
7.82	8.00	0.699	0.120	9.2347-10	3.2660	1845
7.88	8.06	0.301	0.120	9.6006-10	3.8019	6340

a. See reference 42.
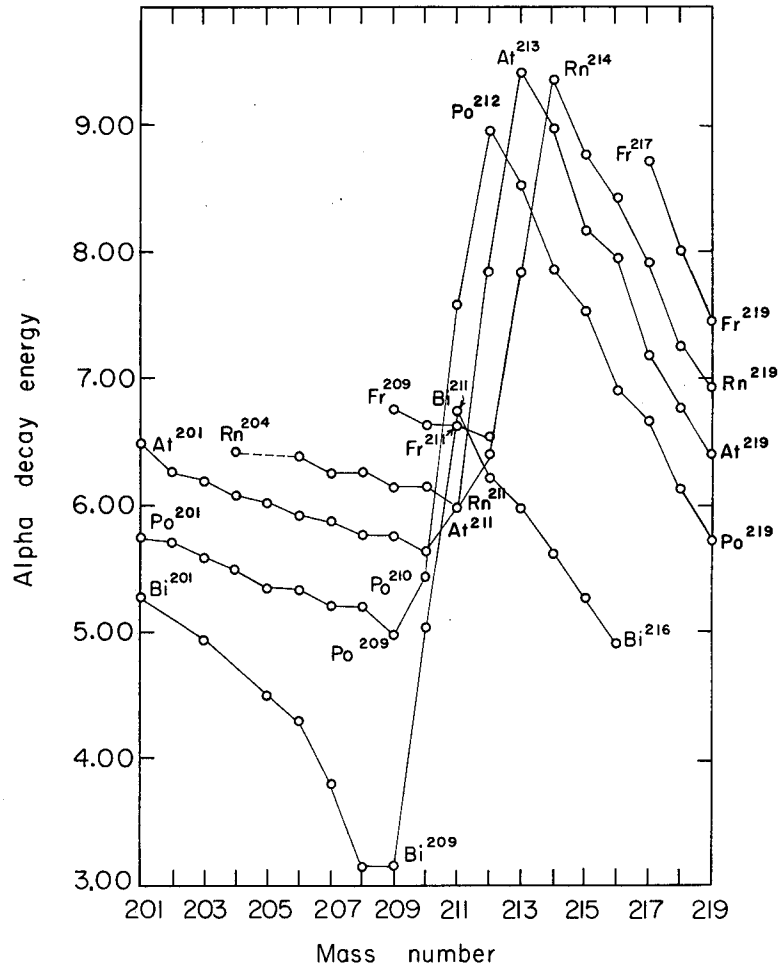
Fig. 23. Graph of alpha-decay energy versus mass number for atomic numbers of 83, 84, 85, 86, 87, and 88.

H. Comparison of Experimental Results
to Cross-Section Predictions

We assume that the total reaction cross section is essentially that of compound-nucleus formation. Innumerable experiments substantiate this assumption for the energy region from 16 to 25 MeV.[10,11,74] Calculations were performed on an IBM 650 computer, using a program designated as Bunthorne Parabolic.[75] This program calculates the transmission coefficients for penetration of the potential barrier seen by a charged particle near the nucleus. We assume that the potential can be approximated by a parabola. Hill and Wheeler[76] have shown that the parabolic potential leads to transmission coefficients of the form[76]

$$T = \frac{1}{1 + \exp\dfrac{2\pi(B - E)}{\hbar w}} \quad ,$$

where B is the barrier height, E is the energy of the system, and w is the vibrational frequency of the harmonic oscillator having a potential-energy function given by the negative of the potential-energy function describing the barrier. Thus, if $V(R)$ is this function describing the barrier, then we have

$$\hbar w = \left[\frac{\hbar}{\mu} \frac{d^2 V}{dR^2}\right]^{1/2}$$

evaluated for that value of R for which $V(R)$ is a maximum (μ is the reduced mass of the system). In the calculations, we assume a diffused-well model with a radius parameter of 1.08 Fermis and a potential function of the form $V(R) = V_c + V_\ell + V_n$, where V_c represents the Coulomb potential,

$$V_c = \frac{Z_1 Z_2 e^2}{R} \quad ,$$

V_ℓ is the centrifugal potential,

$$V_\ell = \frac{\hbar^2 (\ell)(\ell + 1)}{2R^2} \quad ,$$

and V_n is a nuclear potential of the form proposed by Igo[77] for an alpha particle,

$$V_n = V_o \exp[(R_o - R)/c] \quad .$$

The program finds the value of R for which V(R) is a maximum for the given parameters Z_1, Z_2, μ, ℓ, V_o, R_o, and c, and prints out V_{max}, R, ℓ, and w for all values of ℓ such that V_n is less than 10 MeV. It then calculates and prints out

$$\ell, \ T_\ell, \ \text{and} \ \sigma_\ell = \pi \lambdabar^2 (2\ell + 1)T_\ell$$

for these values of ℓ and selected values of the projectile energy, and finally

$$\sigma = \pi \lambdabar^2 \sum(2\ell + 1)T_\ell$$

and the average value of

$$\langle \ell \rangle = \frac{\sum \ell \sigma_\ell}{\sum \sigma_\ell} \quad .$$

In this case, c is 0.574 Fermi, and V_o is - 66.600 MeV. Additionally, we have

$$R = r_o(A_1^{1/3} + A_2^{1/3})$$

where r_o is 1.08 Fermi, A_1 is 4, and A_2 is 209. Here r_o is smaller than is generally chosen. However, this leads to a total cross section that is quite close to the experimental points and, in addition, the r_o around a doubly closed shell (Pb^{208}) should prove to be much smaller than the average r_o.[78]

Results of these calculations are shown in Fig. 24.[79] It is readily seen that there is a very close fit to the experimental data. The experimental data have been accumulated by summing all of the reaction cross sections of the (α, xn) reactions for the projectile energies under study.
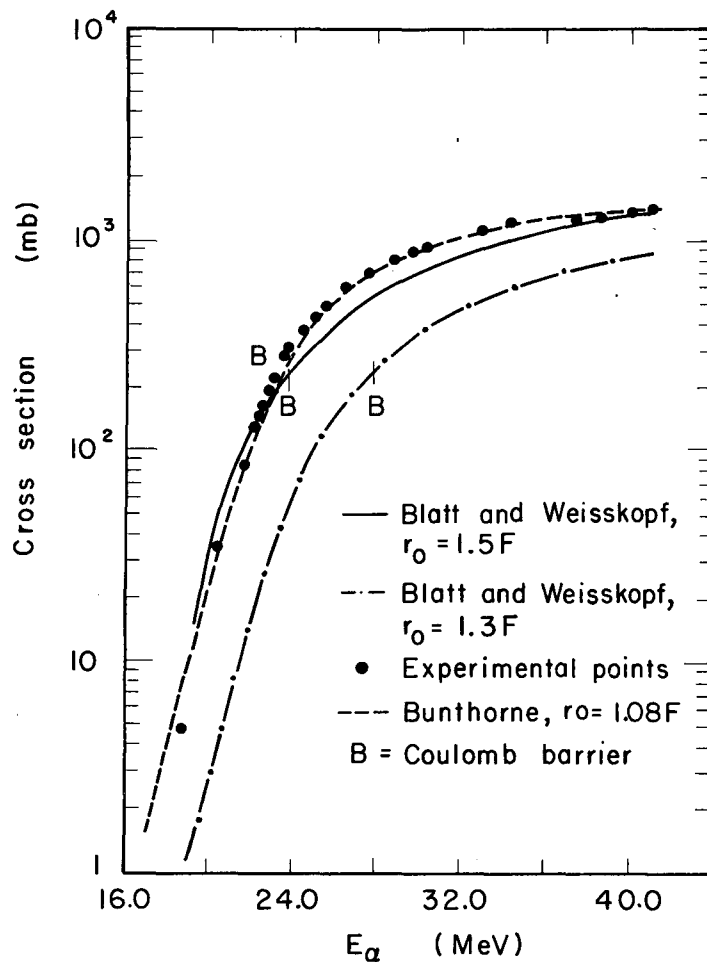
MU-33592

Fig. 24. Cross section for formation of a compound nucleus, based on calculations from Blatt and Weisskopf for r_o of 1.3F and 1.5F and the Bunthorne Parabolic program for r_o of 1.08F. The experimental points are plotted for the summed $Bi(\alpha, xn)At$ cross sections for comparison. The incident-particle energies are from 16 to 44 MeV.

Figure 25 shows the various reaction cross sections as a function of projectile energy, and Fig. 26 shows σ_ℓ as a function of projectile energy.

I. Isomerism

The initial success of the shell model in explaining nuclear isomerism involves the description of single-particle levels that differ by three or more units of angular momentum.[80] There exists a type of isomerism that has not been discussed as a general type. This is isomerism due to the interaction energy between a proton and a neutron in an odd-odd nucleus. Two examples are Bi^{210} and Sc^{42}; it is not coincidental that these are two cases of a single proton and a single neutron outside doubly closed shells. This case (an extra proton and an extra neutron) is a very clear example of the coupling of two nucleons to form a high- or low-spin state. The problem of why the high- and low-spin configurations are the lower-lying levels has been analyzed theoretically by Kim[28] and others,[29] who concluded that a tensor interaction could explain it. This problem is not investigated here, although much data should be obtained to systematize the problem, and many investigations could and should be undertaken to establish the validity of the proposed interacting forces.

Recently, much interest has been focused on the relative yield of isomers in a nuclear reaction as a function of bombardment energy.[81] Although the predictions made in the above references are valid and significant for most cases of nuclear isomerism, they are only partially accurate for the particular examples in odd-odd nuclei. The predictions are valid when the decaying nucleus undergoes gamma de-excitation such that (1) the excitation energy after neutron evaporation and before gamma emission is in the continuum or well above the region where single-particle discrete states can be separated, or (2) the excitation energy does not raise the single particles (proton or neutron) to higher energy levels where the predictions of the statistical model may not be valid. For example, the single-particle levels of protons and neutrons beyond
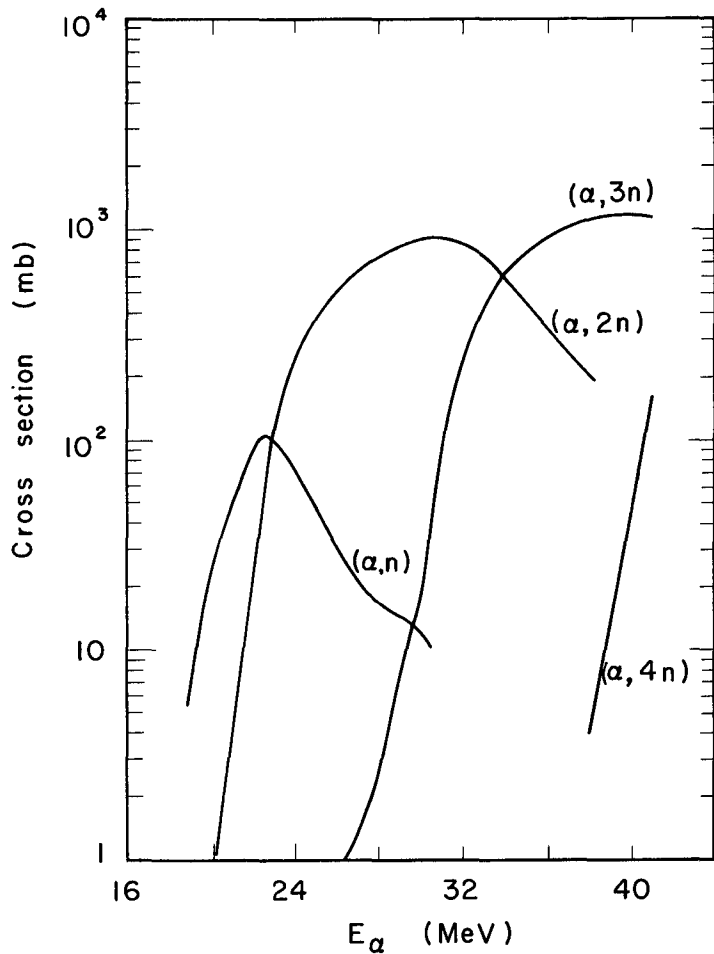
MU-33572

Fig. 25. Cross sections for (α,n), $(\alpha,2n)$, $(\alpha,3n)$, and $(\alpha,4n)$ on bismuth for incident-particle energies from 16 to 44 MeV. Data are taken from this work, Kelly and Segrè,[1] and Ramler et al.[2]
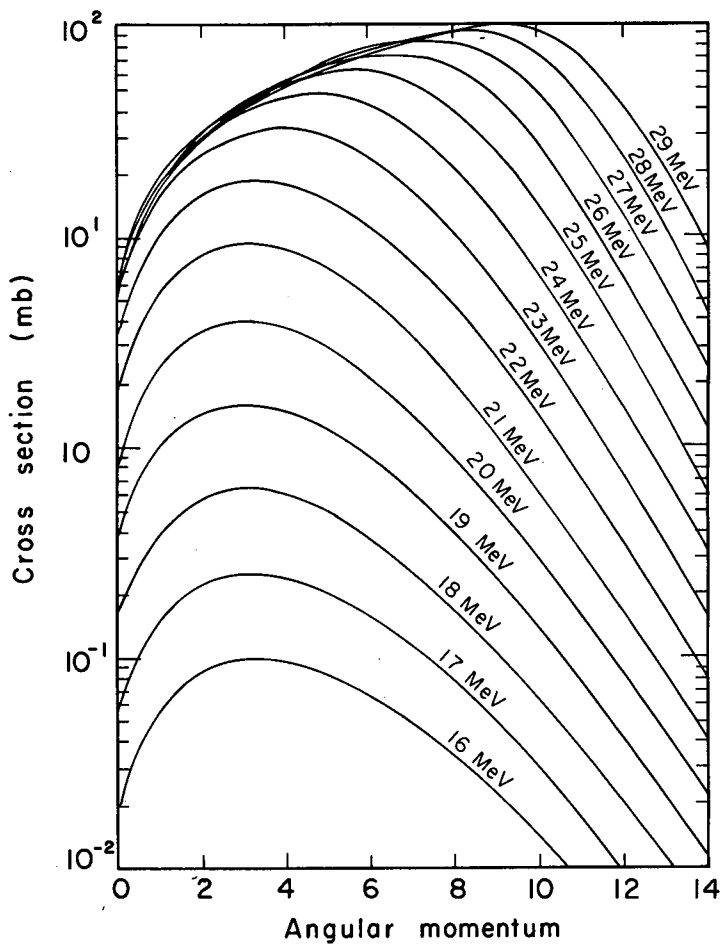
Fig. 26. Calculated cross sections vs angular momentum (1) for
particle energies from 16 through 29 MeV in 1-MeV steps.
These calculations are based on the Bunthorne Parabolic
program.

Pb^{208} are $h_{9/2}$ and $g_{9/2}$, but the first excited state of Pb^{209} is $i_{11/2}$, and the first excited state of Bi^{209} is $f_{7/2}$.[80] Thus, as the particles are given energy and raised to higher levels than the $h_{9/2}$ and $g_{9/2}$, then the $f_{7/2}$, $s_{1/2}$, $d_{3/2}$, and $g_{7/2}$ levels are occupied. Many of these levels do not lead to higher angular momentum of the decaying nucleus. Consequently, in many of these combinations, the total angular momentum may not result in high-spin states, but are restricted to angular-momentum states less than $J = 8$. Thus, if Kim's energy levels of Bi^{210} (Fig. 27) are used as a basis for the order of the levels of At^{212}, the γ cascade may be predominantly to the low- and not the high-spin state at limited bombardment energies.

A demonstration of this phenomenon is presented in Wing's curves on isomeric yield ratios.[81] Almost all the odd-odd isomers have yield curves as a function of energy that peak and then drop off, whereas this is not true in the odd-A cases. Looking at the exceptions to this argument, we see that the ground state of In^{114} resulting from the (p,n) reaction on Cd^{114} should be $(d_{3/2},p_{1/2})$,[80] and the high-spin states should be $(s_{1/2},g_{9/2})$, $(d_{3/2},g_{9/2})$, and $(h_{11/2},g_{9/2})$. Therefore the production of the high-spin state is a statistical problem and should increase in the continuum. The $Se^{80}(d,2n)Br^{80}$ is also a case where $(p_{1/2},p_{3/2})$ is the ground state, and the excited states are $(g_{9/2},p_{3/2})$ or $(g_{9/2},f_{5/2})$. The $Nb^{93}(\alpha,3n)Tc^{94}$ reaction should go to $(g_{9/2},f_{5/2})$ as the ground state, and the excited states should be $(g_{9/2},g_{7/2})$ or $(g_{7/2},d_{5/2})$. Thus, here also there is a change of single-particle energy levels for the isomeric states. These cases do not represent odd-odd-nucleon interaction coupling energy.

With the above arguments in mind, one may follow the Vandenbosch-Huizenga (V-H) model to the point where the ratio breaks away from their predicted curves. Applying the Bunthorne calculations of total cross section, one finds the isomeric ratio

$$R = \frac{\sum\limits_{j=k}^{n} \sigma_j}{\sum\limits_{i=0}^{i=k} \sigma_i}$$
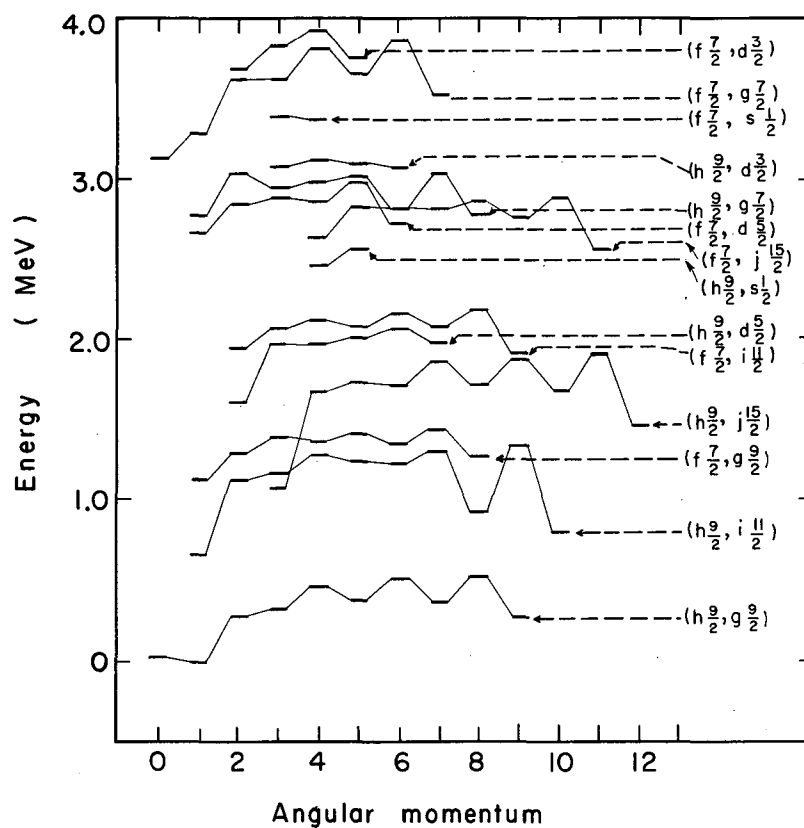
Fig. 27. Calculated energy levels of Bi^{210} from Kim.[28]

where k is the cutoff for the production of the low-spin state. All the orbital angular-momentum transfers greater than k contribute to the high-spin state and all cases where less than k units of angular momentum are transferred contribute to the low-spin state. So, up to the point where the experimental data breaks away from the V-H predictions (see Fig. 28) and $\Delta \ell$ is greater than 3, the high-spin state is favored. However, for $\Delta \ell \leqq 3$ the low-spin state is favored. At 24 MeV the ratio begins to deviate markedly from the V-H predictions.

J. Energy Levels

Application of Kim's results[28] for Bi^{210} to At^{212} can not be quantitatively justified. The results do permit a first-order approximation. The levels of Bi^{210}, predicted by Kim, are shown in Fig. 27. Applying his reasoning, one can state that if the excitation energy does not exceed the pairing energy for the $(h_{9/2})^2_0$, then the core can be increased to include this extra pair of nucleons. So, if the investigation is limited to energy levels below this pairing energy, we can assume that this pair is inert and not responsive to small energy changes.

A study of the energy levels of Po^{210} shows that the pairing energy of $(h_{9/2})^2_{J=0,2,4,6}$ protons is as follows:

0+	ground state	0.0 MeV
2+		1.18 MeV
4+		1.43 MeV
6+		1.48 MeV .

Thus, if levels below 1.18 MeV are investigated, the $(h_{9/2})^2_0$ pair should be intact and the paired energy of these protons is not disturbed, so they can be considered as part of the inert core.

The levels of At^{212} should be as follows:

1-	ground state	0.0 MeV
0-		0.040 MeV
9-		0.220 MeV
2-,3-,4-,5-,6-,7-,8-	from 0.250 to 0.550 MeV	

(with 8- being the highest energy state).
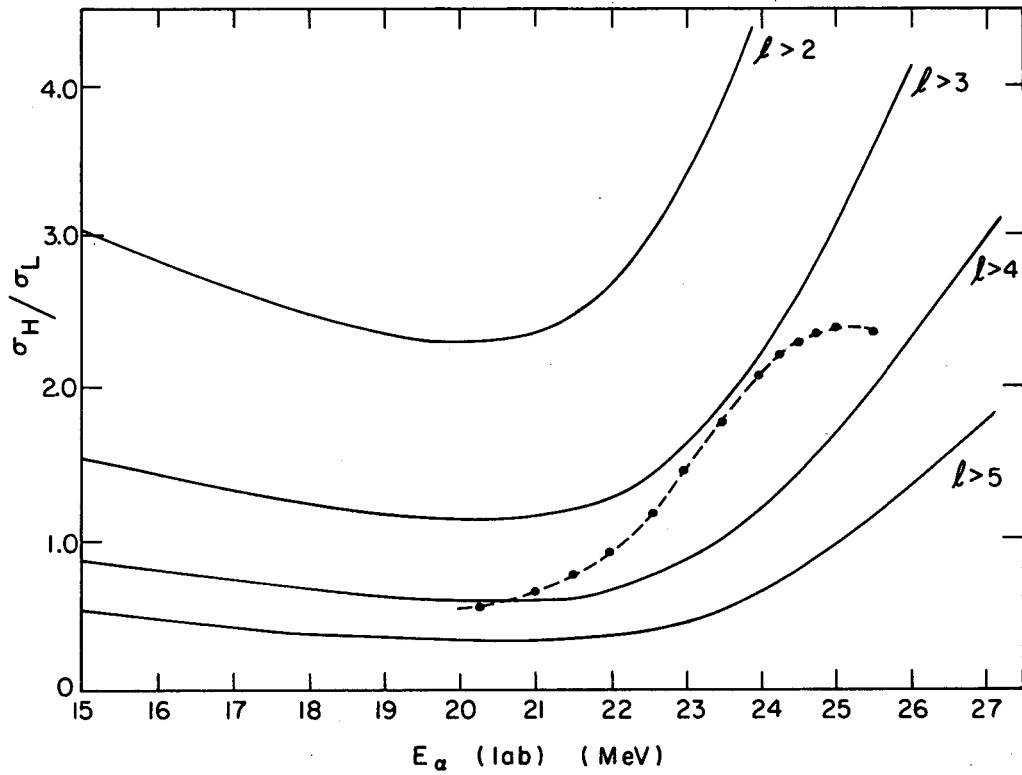
Fig. 28. Ratio of cross section for high- to low-spin state versus incident-particle energy as a function of various cutoffs for production of the high-spin state. The calculated values (solid curves) are from the Bunthorne Parabolic program; the experimental values are given in the dashed curve.

K. Excitation Energy of the Compound Nucleus
and the Threshold for a Reaction

The excitation energy, E^*, of the compound nucleus is defined by

$$E^* = Q + E_L - R_r ,$$

where E_L is the laboratory energy of the incoming particle, and E_r is the recoil energy of the compound system. Thus we have

$$E^* = Q + \frac{M}{m + M} E_L ,$$

where M is the mass of the system, and m is the mass of the incident particle.

To determine the threshold for the (α,n) reaction, we use the mass relation

$$_2He^4 + _{83}Bi^{209} \rightarrow _{85}At^{212} + n_o + Q' .$$
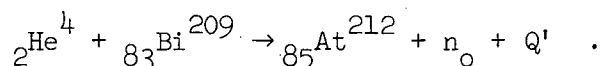
We assume that the neutrons have zero kinetic energy. Using Seegar's determinations[82] as a basis for the calculations, we find that Q' is 14.0 MeV. This value is very close to the 13.7-MeV Q' determined from the mass relation given by Foreman.[32] The closed energy-cycle calculations give 15.2 MeV for the threshold of the reaction, based on 7.43 MeV as the binding energy for a neutron in Bi^{209}.[61]

The Coulomb barrier is calculated from the relation

$$E_b = \frac{Z_1 Z_2 e^2}{R} ,$$

where Z_1 and Z_2 are the charges of the incident particle and the nucleus, respectively (for this case Z_1 is 2; Z_2 is 83), and R is the distance between their centers when they are in contact. For our case, E_b is 22.8 MeV.

No reaction is possible below the threshold energy, and the incident particle must penetrate the Coulomb barrier. In this case, the reaction threshold is below the Coulomb barrier; thus, there is barrier penetration.

Figure 24 shows the total cross section σ for compound-nucleus formation in the bombardment of bismuth with alpha particles as a function of incident-particle energy. The bar B indicates the Coulomb-barrier height, as calculated above, based on the r_o assigned to each curve. The curve marked B and W is from Blatt and Weisskopf,[79] the other curve is from the Bunthorne Parabolic potential,[75] and the circled points are the experimental results of this work added to those reported by Kelly[1] and Ramier.[2]

Figure 25 shows the cross sections for the various products as a function of the energy of the incident alpha particle. The yield of products resulting in charged-particle emission has been neglected, because their cross sections are so much smaller than those for neutron emission because of the Coulomb barrier against charged-particle emission. The proton Coulomb barrier is 11.4 MeV, and in referring to Jackson's paper,[83] the relative probability of proton emission to neutron emission is much less than 0.05 until the excitation energy for the compound nucleus is greater than 50 MeV. In this investigation, the compound nuclear energies are always less than 12 MeV.

L. Cross Sections for $Bi^{209}(\alpha,n)At^{212}$
Based on the Jackson Model

To calculate the cross section for the $Bi^{209}(\alpha,n)At^{212}$ reaction, the neutron-energy distribution as given in the section on cross-section determinations in this paper is used as a basis. This probability of emission of a neutron of energy T leads to the probability of emission of x number of neutrons $P(E,x)$ as a function of the incident particle energy E,

$$P(E,x) = I(\Delta_x, 2x-3) - I(\Delta_x, 2x-1) .$$

Here Δ_x is $(E - \Sigma B_i)/\tau$, where B_i is the binding energy of the $i\underline{th}$ neutron, τ is the nuclear temperature, and

$$I(z,n) = \frac{1}{n!} \int_0^z y^n e^{-y} dy .$$
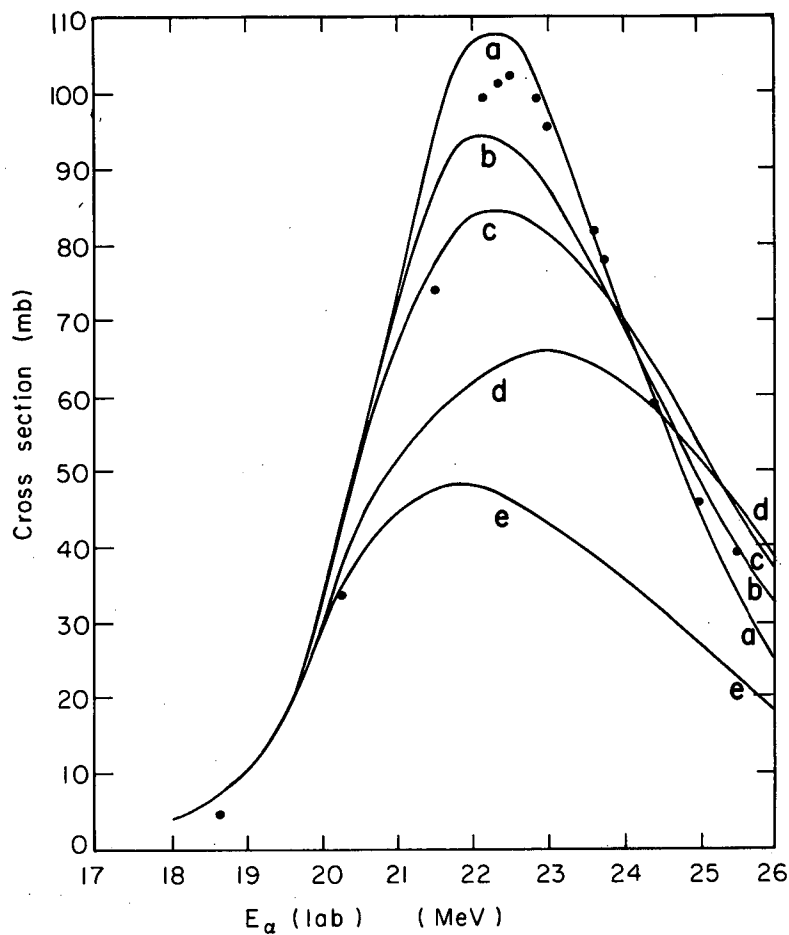
This results in a cross section

$$\sigma(\alpha,n) = \sigma_c(E) \sum_{i=0}^{1} q(i,0)\langle P(E,x-i)\rangle \quad ,$$

where $\sigma_c(E)$ is the reaction cross section for an incident alpha particle
of energy E. Energy (E) can be calculated by using reaction theory.
We calculated the values for $\sigma_c(E)$ by using (a) Blatt and Weisskopf for
r_o = 1.5 Fermi, and (b) the Bunthorne parabolic calculations for the
Hill-Wheeler[76] potential and r_o = 1.08 Fermi.

The nuclear temperatures and the binding energies of the neutrons
(which determine the Q of the reaction) can be varied. The Q values
cannot be varied over a wide range, inasmuch as they have been determined
from experimental data within 1.5 MeV. Figures 29 and 30 show how sensitive
the cross section is to changes in Q. For a change of 1 MeV the peak of
the reaction moves almost the same amount. The nuclear temperature is
calculated from the relationship, $\tau = (aE)^{1/2}$, where a is a constant
related to the level density and has a value of approximately 0.1 MeV
for heavy elements.[84] This results in a nuclear temperature of
1.0 MeV $\leq \tau \leq$ 1.8 MeV, and so we have used values of 1.0, 1.2, 1.4, and
1.8 MeV to demonstrate the dependence of the cross section upon this
parameter. Over the range of energies that the reaction is investigated,
the nuclear temperature can be considered to be a constant.

Figure 29 compares results of the Bunthorne Parabolic program (which
has been outlined in Section IV, Discussion) to the experimental results
for different Q values and nuclear temperatures. Figure 30 shows the
comparison of the Blatt-Weisskopf predictions for several nuclear temper-
atures and Q values to the experimental results.

Agreement between calculated and experimental values is quite good
for a nuclear temperature of 1.0 MeV and a Q of 21.1 MeV for the $(\alpha,2n)$
reaction. These values are reasonably close to the estimated nuclear
temperature and Q.[60]

Cross section (mb)

110
100
90
80
70
60
50
40
30
20
10
0

a
b
c
d
e

d
c
b
a
e

17 18 19 20 21 22 23 24 25 26

E_α (lab)   (MeV)

MU-33595

Fig. 29.   Calculated cross sections for the $Bi(\alpha,n)At$ reaction
for incident-particle energies from 18 through 26 MeV for
various values of nuclear temperature (T) and Q for the
reactions used in these calculations.   These curves are
based on a Hill-Wheeler potential; Bunthorne program
calculations are used.   Experimental results are shown
as circled dots.
(a)   T = 1.0 MeV, $Q(\alpha,2n)$ = 21.1 MeV;
(b)   T = 1.2 MeV, $Q(\alpha,2n)$ = 20.6 MeV;
(c)   T = 1.4 MeV, $Q(\alpha,2n)$ = 20.1 MeV;
(d)   T = 1.8 MeV, $Q(\alpha,2n)$ = 18.8 MeV;
(e)   T = 1.4 MeV, $Q(\alpha,2n)$ = 18.8 MeV.
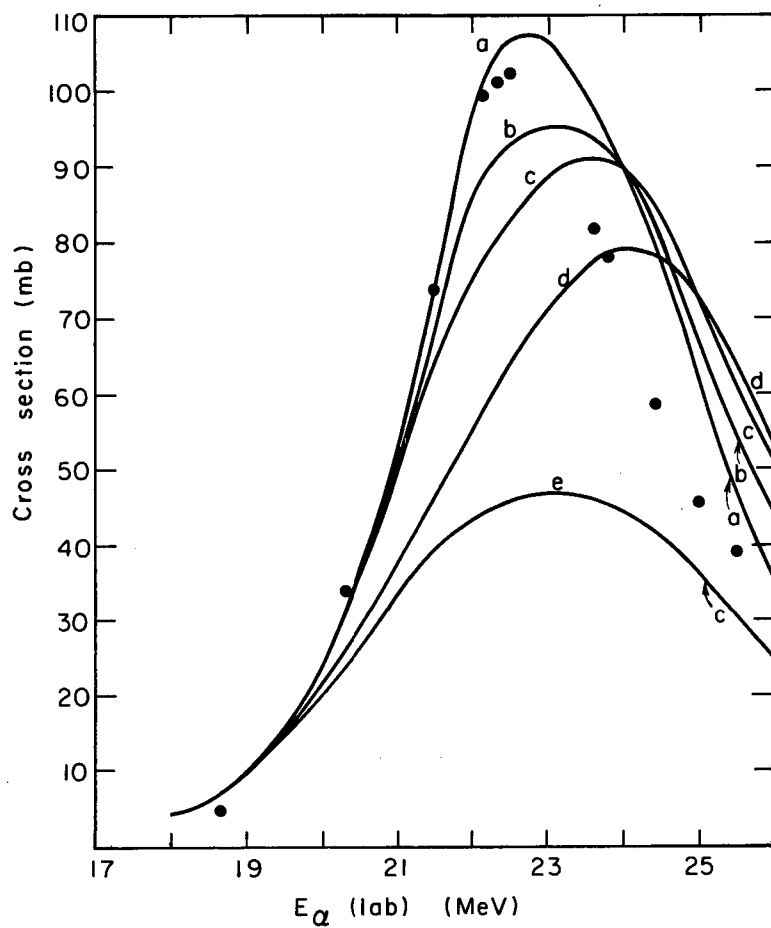
Fig. 30. Calculated cross sections for the same reaction as in Fig. 29 but based on the Blatt and Weisskopf[84] r_o of 1.5F.

(a) T = 1.0 MeV, $Q(\alpha,2n)$ = 21.1 MeV;
(b) T = 1.2 MeV, $Q(\alpha,2n)$ = 20.6 MeV;
(c) T = 1.4 MeV, $Q(\alpha,2n)$ = 20.1 MeV;
(d) T = 1.8 MeV, $Q(\alpha,2n)$ = 18.8 MeV;
(e) T = 1.4 MeV, $Q(\alpha,2n)$ = 18.8 MeV.

V. CONCLUSIONS

1. There is a high-spin isomeric state of At^{212} at an excitation energy of 220±20 keV.

    a) The decay mode, pure alpha decay with no γ-de-excitation, suggests at least four units of angular momentum difference between the isomer and the ground state.

    b) The hindrance to decay suggests that the isomeric state is as many units of angular momentum away from four (4+) or five (5+) (the ground state of Bi^{208}) as the ground state.

    The ground state of At^{212} cannot have zero spin, as it decays to both the 4+ and 5+ states of Bi^{208}. Following the suggestions of Kim and others for the energy levels of Bi^{210}, these data lead one to assign 1- and 9- for the spins of the states of At^{212} observed.

2. The Vandenbosch-Huizenga (V-H) model cannot be satisfactorily applied to describe the isomeric cross section ratios of odd-odd nuclei at low excitation. This conclusion could be expected, inasmuch as the V-H assumption is statistically based and this is not the region of validity for that assumption. The V-H system has been successful in describing the isomeric cross-section ratios for many cases not within the region of validity, so one should try to understand the reason for this failure. It is proposed that the failure is due to nonvalidity of the fundamental assumption of the single particle state level description of isomerism when applied to these odd-odd isomers.

3. Energy levels and the associated spin assignments of odd-odd nuclei should be investigated systematically, particularly near doubly closed shells and high-spin single particle states, to give more data for a better understanding of the nature of nuclear forces.

4. The total reaction cross section of alpha particles on bismuth from 15 to 30 MeV can be accounted for within the concept of the formation of the compound nucleus; however, there appears to be discrepancies in the choice of radius of interaction when compared to other nuclear reactions. These discrepancies can be understood if one accepts a "shrinking" of interaction radius at the doubly closed shell.

VI. ACKNOWLEDGMENTS

VII. REFERENCES

1. E. L. Kelly and E. Segrè, Phys. Rev. 75, 999 (1949).

2. W. J. Ramler, J. Wing, D. H. Henderson, and J. R. Huizenga, Phys. Rev. 114, 154 (1959).

3. P. F. Donovan, B. G. Harvey, and W. H. Wade, Phys. Rev. 119, 218, 225 (1960).

4. W. H. Wade, J. Gonzalez-Vidal, R. A. Glass, and G. T. Seaborg, Phys. Rev. 107, 1311 (1957).

5. J. R. Huizenga, R. Chandry, and R. Vandenbosch, Phys. Rev. 126, 210 (1962).

6. M. Weissbluth, T. M. Putnam, and E. Segrè (unpublished work) reported by D. Strominger, J. M. Hollander, and G. T. Seaborg, Rev. Mod. Phys. 30, 585 (1958).

7. M. M. Winn, Proc. Phys. Soc. (London) A67, 949 (1954).

8. J. C. Ritter and W. G. Smith, Phys. Rev. 128, 1778 (1962); R. G. Griffioen and R. D. Macfarlane, in Lawrence Radiation Laboratory Report UCRL-10023, January 1962.

9. N. Bohr, Nature 137, 334 (1936).

10. S. Ghoshal, Phys. Rev. 80, 939 (1950).

11. W. John, Jr., Phys. Rev. 103, 704 (1956).

12. J. F. Mollenauer, Lawrence Radiation Laboratory Report UCRL-9724, June 1960.

13. G. N. Simonoff and J. M. Alexander, Lawrence Radiation Laboratory Report UCRL-10099, 1962.

14. J. M. Alexander and G. N. Simonoff, Lawrence Radiation Laboratory Report UCRL-10541, 1963.

15. R. Vandenbosch and J. R. Huizenga, Phys. Rev. 120, 1313 (1960).

16. F. Fukuzawa, J. Phys. Soc. (Japan) 16, 2371 (1961).

17. E. Weigold and R. N. Glover, Nucl. Phys. 32, 106 (1962).

18. T. Ericson and V. M. Strutinsky, Nucl. Phys. 8, 284 (1958); 9, 689 (1959).

19. P. C. Gugelot, Phys. Rev. 81, 51 (1951).

20. O. Hahn, Chem. Ber. 54, 1131 (1921).

21. B. V. Kurchatov, I. Kurchatov, L. Myssowski, and L. Roussinow, Comptes Rendus 200, 1201 (1953).

22. C. F. Weizsäcker, Naturwiss. 24, 813 (1936).

23. E. Segrè and A. C. Helmholz, Rev. Mod. Phys. 21, 271 (1949).

24. C. T. Bishop, Argonne National Laboratory Report ANL-6405, 1961.

25. L. W. Nordheim, Phys. Rev. 78, 294 (1950).

26. A. de-Shalit, Phys. Rev. 91, 1479 (1953).

27. D. Kurath, Phys. Rev. 91, 1430 (1953); D. M. Brink, Proc. Phys. Soc. (London) A67, 757 (1954); S. P. Pandya, Phys. Rev. 108, 1312 (1957); N. D. Newby, Jr. and E. V. Konopinsky, Phys. Rev. 115, 434 (1959).

28. Y. E. Kim and J. O. Rasmussen, Nucl. Phys. 47, 184 (1963); Y. E. Kim (Thesis), Lawrence Radiation Laboratory Report UCRL-10865, 1963.

29. P. A. Mello and J. Flores, Nucl. Phys. 47, 177 (1963).

30. R. A. Glass, S. G. Thompson, and G. T. Seaborg, J. Inorg. Nucl. Chem. 1, 3 (1955).

31. K. Way and M. Wood, Phys. Rev. 94, 119 (1954).

32. B. M. Foreman, Lawrence Radiation Laboratory Report UCRL-8223, 1958.

33. G. Gamow, Zeit. Phys. 51, 204 (1928); E. U. Condon and R. W. Gurney, Nature 122, 439 (1928).

34. H. A. Bethe, Rev. Mod. Phys. 9, 69, 170 (1937).

35. G. H. Winslow, Phys. Rev. 96, 1032 (1954).

36. R. G. Thomas, Progr. Theor. Phys. 12, 253 (1954).

37. H. Mang, Zeit. Phys. 148, 582 (1957); Phys. Rev. 119, 1069 (1960).

38. H. D. Zeh and H. Mang, Nucl. Phys. 29, 529 (1962).

39. J. O. Rasmussen, Phys. Rev. 113, 1593 (1959); 115, 1675 (1959).

40. K. Harada, Progr. Theor. Phys. 26, 667 (1961).

41. M. A. Preston, Physics of the Nucleus (Addison-Wesley, New York, 1962), Ch. 14.

42. C. J. Gallagher and J. O. Rasmussen, J. Inorg. Nucl. Chem. 3, 333 (1957).

43. G. E. Fischer, Phys. Rev. 96, 704 (1954).

44. R. E. Ellis, Lawrence Radiation Laboratory Report UCRL-3114, August 1955.

45. K. D. Jenkins and W. B. Jones, Rev. Sci. Instr. 29, 898 (1958).

46. F. S. Goulding and W. L. Hansen, Lawrence Radiation Laboratory Report UCRL-9436, 1960.

47. C. Williamson and J. P. Boujot, "Tables of Range and Rate of Energy Loss of Charged Particles of Energy 0.5 to 150 MeV," unpublished report, Centre d'Études Nucleaires Saclay, 1962.

48. W. W. Goldsworthy, Lawrence Radiation Laboratory Report UCRL-9816, 1961.

49. J. L. Blankenship and C. J. Borkowski, IRE Trans. Nucl. Sci. 7, 190 (1960).

50. B. G. Harvey, E. J. M. Rivet, A. Springer, J. R. Meriwether, W. B. Jones, J. H. Elliott, and P. Darriulat, Lawrence Radiation Laboratory Report UCRL-10727, 1963, to be published in Nucl. Phys.

51. L. E. Miles, G. L. Wigle, P. A. Bohm, R. G. Altes, T. C. Parsons, and P. W. Howe, Lawrence Radiation Laboratory Report UCRL-10368, 1962.

52. This energy was determined by cyclotron parameters and verified by checking the excitation functions obtained against those obtained at the 60-Inch Cyclotron.

53. R. M. Diamond, B. Elbek, and F. S. Stephens, Nucl. Phys. 43, 560 (1963).

54. B. Elbek and M. Nakamura, Nucl. Instr. 10, 164 (1961).

55. R. M. Diamond, Lawrence Radiation Laboratory, Berkeley, private communication, 1963.

56. R. D. Evans, The Atomic Nucleus (McGraw-Hill, New York, 1955), p. 812.

57. R. W. Hoff, Instruction Sheet (mimeo) for Frenic, Lawrence Radiation Laboratory, Berkeley, California.

58. J. R. Morton (Thesis), Lawrence Radiation Laboratory Report UCRL-9595, 1961.

59. J. M. Alexander and L. Winsberg, Phys. Rev. 121, 518, 529 (1959) and J. M. Alexander and D. H. Sisson, Lawrence Radiation Laboratory Report UCRL-10098, 1962.

60. P. M. Endt and M. Demeur, Nuclear Reactions (North Holland Publishing Co., Amsterdam, 1961), Vol. 1, p. 331.

61. Nuclear Data Sheets (July 1963), compiled by K. Way et al. (National Academy of Sciences, National Research Council, U. S. Government Printing Office, Washington, D.C.).

62. M. E. Rose, Internal Conversion Coefficients (North Holland Publishing Co., Amsterdam, 1958).

63. D. H. Templeton, J. J. Howland, and I. Perlman, Phys. Rev. 72, 758, 766 (1947).

64. F. N. Spiess, Phys. Rev. 94, 1292 (1954).

65. D. Strominger, J. M. Hollander, and G. T. Seaborg, Lawrence Radiation Laboratory Report UCRL-1928 rev., 1958.

66. G. Friedlander and J. W. Kennedy, Nuclear and Radiochemistry (John Wiley, New York, 1955).

67. B. G. Harvey, Introduction to Nuclear Physics and Chemistry (Prentice-Hall, Englewood Cliffs, N. J., 1962).

68. M. H. Brennan and A. M. Bernstein, Phys. Rev. 120, 927 (1960).

69. P. Mukherjee and B. L. Cohen, Phys. Rev. 127, 1284 (1962).

70. J. M. Blatt and V. Weisskopf, Theoretical Nuclear Physics (John Wiley and Sons, New York, 1952), p. 571.

71. P. Mukherjee, Phys. Rev. 131, 2162 (1963).

72. S. Wahlborn, Nucl. Phys. 3, 644 (1957).

73. E. Segrè, Ed., Experimental Nuclear Physics (John Wiley and Sons, New York, 1959).

74. P. Donovan (Thesis), Lawrence Radiation Laboratory Report UCRL-8347, 1958.

75. "Bunthorne Parabolic Calculations" (mimeo), Lawrence Radiation Laboratory.

76. D. L. Hill and J. A. Wheeler, Phys. Rev. 89, 1102 (1953).

77. G. Igo, Phys. Rev. Letters $\underline{1}$, 72 (1958) and Phys. Rev. $\underline{115}$, 1665 (1959).

78. R. H. Pehl, Lawrence Radiation Laboratory, Berkeley, private communication, 1963.

79. J. M. Blatt and V. Weisskopf, op. cit., p. 352.

80. M. G. Mayer and J. H. D. Jenson, <u>Elementary Theory of Nuclear Structure</u> (John Wiley and Sons, New York, 1955), Ch. 13.

81. J. Wing, Argonne National Laboratory Report ANL-6598, 1962; D. W. Seegmiller, Lawrence Radiation Laboratory Report UCRL-10850, 1963; R. Kiefer, Lawrence Radiation Laboratory Report UCRL-11049, 1963.

82. P. A. Seegar, Nucl. Phys. $\underline{25}$, 1 (1961).

83. J. D. Jackson, Can. J. Phys. $\underline{34}$, 767 (1956).

84. J. M. Blatt and V. Weisskopf, op. cit., pp. 371, 372.